Mechanical Systems and Signal Processing 220 (2024) 111677

Contents lists available at ScienceDirect

Mechanical Systems and Signal Processing

journal homepage: www.elsevier.com/locate/ymssp

Investigation of time-varying frequencies of two-axle vehicles and bridges during interaction using drive-by methods and improved multisynchrosqueezing transform

Zhenkun Li [a,*], Yifu Lan [a], Kun Feng [b], Weiwei Lin [a]

[a] Department of Civil Engineering, Aalto University, 02150 Espoo, Finland
[b] School of Mechanical and Aerospace Engineering, Queen's University Belfast, BT7 1NN Belfast, UK

ARTICLE INFO

Communicated by H. Ouyang

Keywords:
Bridge structure
Vehicle–bridge interaction
Drive-by method
Time–frequency representation
Multisynchrosqueezing transform

ABSTRACT

Recent studies have highlighted the superiority of the drive-by method using vehicle responses to identify bridge frequencies due to its cost-effectiveness. However, most research identifies bridge and vehicle frequencies as time-invariant, which neglects the non-stationary nature of vehicle–bridge interaction systems. This assumption holds true only when the vehicle's mass is significantly less than that of the bridge. With an increase in vehicle–bridge mass ratio, relying on this assumption can lead to substantial errors, necessitating an investigation of time-varying characteristics extracted from vehicle responses. This study extends this exploration to extract time-varying frequencies of a vehicle–bridge interaction system involving a two-axle vehicle and a bridge through the drive-by method and improved multisynchrosqueezing transform. The semi-analytical solution for time-varying frequencies is newly derived, and numerical simulations are employed to verify the solution and the effectiveness of the improved multisynchrosqueezing transform. Various influencing factors, including vehicle speed, vehicle damping, bridge damping, stiffness of the bridge and vehicle, environmental noises, and road roughness, are analyzed. Additionally, laboratory experiments with a scaled two-axle vehicle and two bridge models are conducted to verify the proposed method, and case studies on different parameters are further provided. Results demonstrated that the time-varying bridge frequency can be extracted from vehicle responses using the proposed approach. Finally, a novel index is proposed to evaluate the extraction results of the bridge's time-varying frequency from vehicle responses.

1. Introduction

Bridge structures are of critical importance in the global transportation system [1]. However, many bridges, especially those in Europe and America, have been in service for a significant number of years and may face issues related to aging and deterioration [2,3]. To ensure their safe operation, researchers have turned their attention to condition assessment of bridges in recent decades. Vibration-based approaches have emerged as a promising strategy due to their convenience and ease of operation [4]. These methods typically analyze the modal parameters of bridges and examine their changes before and after damage. Among these modal parameters, bridge frequencies, as fundamental indicators, have been widely utilized by researchers [5].

To determine the frequencies of a bridge, it is common practice to install accelerometers on the bridge to collect vibration data for modal analysis, known as the direct method. Once the bridge's responses are obtained, modal analysis can be performed

* Corresponding author.
E-mail addresses: zhenkun.li@aalto.fi (Z. Li), yifu.lan@aalto.fi (Y. Lan), k.feng@qub.ac.uk (K. Feng), weiwei.lin@aalto.fi (W. Lin).

https://doi.org/10.1016/j.ymssp.2024.111677
Received 4 March 2024; Received in revised form 6 June 2024; Accepted 22 June 2024

to determine its frequencies. Modal analysis can be divided into two types: experimental modal analysis and operational modal analysis. However, experimental modal analysis typically requires simultaneous measurements of both the excitation and response, making it less practical for engineering applications. On the other hand, operational modal analysis only requires the output data of the system, making it easier to implement. Nevertheless, operational modal analysis relies heavily on external excitations and can be influenced by environmental and operational variations [6]. Among all operational factors that influence the analysis, traffic flow plays a significant role as it can induce vehicle–bridge interaction (VBI) responses and contribute external energy to bridge vibrations. Previous studies have extensively explored bridge health monitoring using responses under vehicle loads [7,8]. Still, recent research indicates that the direct method often necessitates various sensors to form a sensing network on the bridge, making it costly to implement in engineering, especially considering the increasing number of deteriorating and newly constructed bridges [9].

The interactive nature of the VBI system led to the proposal of the indirect method (also known as the drive-by or vehicle scanning method) to identify bridge frequencies utilizing vehicle responses [10]. Over the last two decades, many studies have focused on identifying bridge frequencies, modal shapes, and damping ratios extracted from vehicle responses [11–13], as well as subsequent missions like damage detection [14–16]. Current research has uncovered two main challenges: firstly, mitigating the impact of road roughness, and secondly, filtering out vehicle information from vehicular responses [17]. Regarding the former, various strategies have been explored and proven effective in mitigating the adverse influence of road roughness. These strategies include the use of residual accelerations from connected vehicles [18], residual frequency spectrum [19], and external excitation sources [20]. Additionally, by back-calculating contact-point responses from the vehicle's accelerations, the bridge's frequencies were highlighted [21]. The indirect approach is heavily dependent on the VBI theories. Notwithstanding, the majority of current studies have treated the bridge's frequencies as fixed values with no time variability, thereby disregarding the non-stationary nature of the VBI system. This assumption holds true only when the vehicle–bridge mass ratio is significantly low [22]. However, existing research indicates that heavy vehicles can potentially enhance bridge vibrations and facilitate indirect bridge information extraction [23]. Under this condition, extracting time-invariant frequency values can lead to substantial errors, particularly when a large vehicle–bridge mass ratio is employed [24]. Hence, it becomes imperative to investigate the time-varying frequencies of the VBI system, as it would offer valuable insights for bridge dynamic information tracking.

Time–frequency analysis (TFA) can provide significant information for analyzing non-stationary signals. Traditional TFA methods, such as the short-time Fourier transform (STFT) and wavelet transform, have been widely employed to determine the instantaneous frequency (IF) of time-varying signals. In 2019, Cantero et al. [25] investigated the application of wavelet transform in analyzing the time-varying frequencies of the VBI system. Although they observed slight changes in the frequency of the beam and vehicles, the time–frequency representations (TFRs) were not clear enough to capture distinct traces of time-varying frequencies. To address this limitation and enhance the analysis of non-stationary signals, various methods have been proposed, such as the S-transform, reassignment method, synchroextracting transform (SET), and synchrosqueezing transform (SST) [26–29]. Mostafa et al. [30] successfully extracted IFs of the Boyne viaduct during the passage of a locomotive with a vehicle–viaduct mass ratio of approximately 20% using the wavelet synchrosqueezing transform. Tang et al. [31] proposed an improved local maximum synchrosqueezing transform to identify concentrated TFRs for an experimental bridge subjected to moving vehicle loads. Xin et al. [32] utilized an enhanced SET-based empirical wavelet transform to identify the IFs of a time-varying traffic-bridge system. Nonetheless, previous studies primarily utilized accelerometers installed on the bridge to determine the bridge's time-varying frequency during the VBI process. Limited research has been conducted on the drive-by method, which involves attaching accelerometers to passing vehicles, to investigate the time-varying frequencies of both the bridge and the vehicle. In 2013, Yang et al. [33] analyzed the frequency variation of the VBI system by employing a spring–mass vehicle model and a simply supported bridge. The closed-form equations were verified by numerical simulations. However, this study did not consider any external influences. In 2020, Li et al. [34] proposed to analyze vehicle responses to identify time-varying frequencies of bridges. They utilized the SET method on both vehicle and bridge responses, successfully tracking the bridge frequencies. However, it was noted that the SET method could introduce errors in mode reconstruction and IF estimation for rapidly changing signals [35]. Subsequently, in 2023, Tan et al. [22] proposed the use of the high-order SST, which enhanced TFRs for signals with significant time-varying characteristics. Nevertheless, these existing studies using the quarter-car model only considered the vehicle's vertical vibrations. Its pitching effects and corresponding improvement in physics on time-varying frequencies of the VBI system are still not clear. Furthermore, recent studies have shown that the high-order SST method is highly sensitive to noise, often yielding unsatisfactory results for signals with heavy noise. Conversely, the recently introduced improved multisynchrosqueezing transform (IMSST) approach offers a more focused representation in both the time and frequency domains compared to the SET and high-order SST methods [36]. It has the potential to be a promising tool for analyzing vehicle responses and tracking frequency variations in the VBI system.

This paper further analyzes nonstationary responses of VBI systems involving a two-axle vehicle and a bridge. The drive-by method was employed to analyze the responses of the passing vehicle in comparison with direct measurements from the bridge. The innovative contributions of this work are four-fold: (1) New semi-analytical solutions for time-varying frequencies of the VBI system are derived and verified by numerical simulations. (2) Frequency amplification ratios of the two-axle VBI system under varying vehicle–bridge frequency and mass ratios are innovatively offered. (3) For the first time, the enhanced algorithm called IMSST is presented as effective in providing clear TFRs for identifying time-varying frequencies of the VBI system, and the effects of various influence factors in numerical simulations and laboratory experiments are analyzed. (4) A novel index, time-free dynamic time warping (T-DTW), is proposed to evaluate the bridge's time-varying frequency extraction results from drive-by measurements. The remainder of this paper is organized as follows. Section 2 introduces semi-analytical solutions for calculating the time-varying frequencies of the two-axle VBI system, as well as the theories for extracting IFs from vehicle responses using

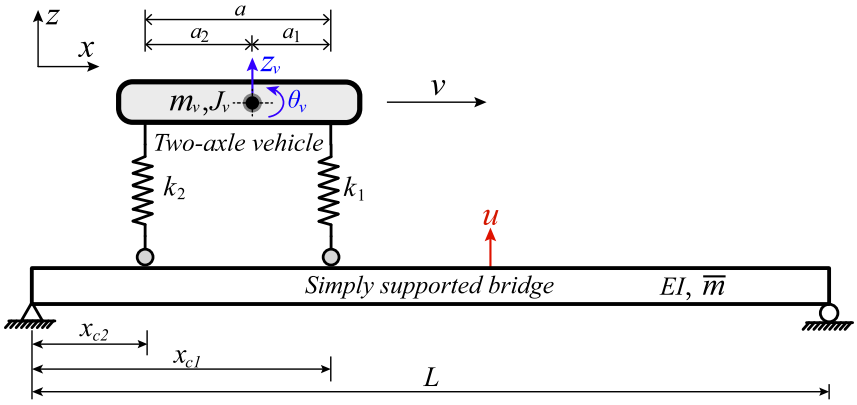

Fig. 1. Analytical model of the two-axle vehicle and bridge.

IMSST. Section 3 presents numerical simulations that verify the accuracy of the semi-analytical solutions and the effectiveness of the time-varying frequency identification using IMSST. Additionally, it includes an analysis of the frequency amplification ratios and various influencing parameters. Section 4 provides an overview of the laboratory experiments conducted using a scaled truck and two beams. It also discusses case studies involving different parameters. Finally, this paper is concluded in Section 5.

2. Theoretical foundation

2.1. Semi-analytical solution for two-axle vehicle–bridge interaction system

The variability of the VBI system, as is widely recognized, leads to varying frequencies of the vehicle and bridge during their interaction [33]. Previous studies have extensively focused on the implementation of the quarter-car model [22,34]. However, in practical scenarios, vehicles often possess more than one axle. Although simplifying the model by employing the quarter-car approach may seem reasonable, it may lead to the loss of crucial information and physical explanations, such as the influence of pitching effects. A commonly adopted alternative is the half-car model, as shown in Fig. 1. In this study, the vehicle is represented by a single mass m_v, which is supported by two springs with respective stiffness values of k_1 and k_2. The moment of inertia of the vehicle body is represented by J_v. The axle distance is a, and its center of gravity is determined by a_1 and a_2. The vehicle encompasses two degrees of freedom (DOFs): the vertical bounce of the body (z_v) and body rotation (θ_v), as indicated by the blue arrows in Fig. 1. On the other hand, the bridge is designed as a simply supported Euler–Bernoulli beam, possessing a length of L, flexural stiffness of EI, and mass per unit length of $\overline{m}$. Throughout the analytical derivation process, the effects of road roughness and damping effects are temporarily ignored and will be analyzed in Section 3.

The equilibrium equations for vibrations of the bridge and two-axle vehicle can be denoted by Eqs. (1)–(3),

$$\overline{m}\ddot{u}(x,t) + EIu(x,t)'''' = \sum_{i=1}^{2} f_{ci}(t)\delta(x - x_{ci}) \tag{1}$$

$$m_v\ddot{z}_v + k_1(z_v + a_1\theta_v - u_{c1}) + k_2(z_v - a_2\theta_v - u_{c2}) = 0 \tag{2}$$

$$J_v\ddot{\theta}_v + k_1a_1(z_v + a_1\theta_v - u_{c1}) - k_2a_2(z_v - a_2\theta_v - u_{c2}) = 0 \tag{3}$$

where $u(x,t)$ denotes the deflection of the bridge. $\dot{(\cdot)}$ means the derivative to time t, and $(')$ represents that to the position on the bridge x. $\delta(\cdot)$ represents the Dirac's delta function. $f_{ci}(t)$ means the contact force between the vehicle and bridge, which can be represented by Eqs. (4) and (5),

$$f_{ci}(t) = k_i(z_{vi} - u_{ci}) - m_{vi}g, i = 1, 2. \tag{4}$$

$$z_{vi} = z_v + (-1)^{i+1}\theta_v a_i, i = 1, 2. \tag{5}$$

where z_{vi} is the ith axle's displacement, and $m_{vi}g = m_v g(a - a_i)/a$ is the axle weight. g is the acceleration of gravity. u_{ci} means the deflection of the beam at the ith contact point. For the beam's vertical deflection, it can be represented by the form of modal superposition. For the reason of simplicity, only the first mode of the beam is considered in the analytical solutions. The beam's deflection $u(x,t)$ can be denoted by Eq. (6),

$$u(x,t) = q_b(t)\sin(\frac{\pi x}{L}) \tag{6}$$

where $q_b(t)$ is the generalized coordinate (t is omitted for simplification later). It is noted that higher modes of the beam can also be included, but it only increases the mathematical complexity and will not contribute to the understanding of physical meaning [33].

However, for the vehicle, it is worth including more DOFs that can help with understanding physical phenomena in practical engineering. By substituting Eq. (6) into Eq. (1), we can get

$$\overline{m}\sin(\frac{\pi x}{L})\ddot{q}_b + \frac{EI\pi^4}{L^4}\sin(\frac{\pi x}{L})q_b = \sum_{i=1}^{2}\left[k_i(z_{vi} - \sin(\frac{\pi x_{ci}}{L})q_b) - m_{vi}g\right]\delta(x - x_{ci}) \tag{7}$$

Note that the Dirac's function exists in Eq. (7). It is multiplied by the modal shape $\sin(\pi x/L)$ and integrated with respect to x from zero to L. After rearranging all items related to $\ddot{q}_b$, q_b, z_v, and θ_v, we can get

$$\left[\frac{\overline{m}L}{2}\right]\ddot{q}_b + \left[\frac{EI\pi^4}{2L^3} + \sum_{i=1}^{2}k_i\sin^2(\frac{\pi x_{ci}}{L})\right]q_b - \left[\sum_{i=1}^{2}k_i\sin(\frac{\pi x_{ci}}{L})\right]z_v - \left[\sum_{i=1}^{2}(-1)^{i+1}k_i a_i\sin(\frac{\pi x_{ci}}{L})\right]\theta_v = -\sum_{i=1}^{2}m_{vi}g\sin(\frac{\pi x_{ci}}{L}) \tag{8}$$

Also, for Eqs. (2) and (3), by substituting Eq. (6) into them, one obtains

$$m_v\ddot{z}_v - \left[\sum_{i=1}^{2}k_i\sin(\frac{\pi x_{ci}}{L})\right]q_b + (k_1 + k_2)z_v + (k_1a_1 - k_2a_2)\theta_v = 0 \tag{9}$$

$$J_v\ddot{\theta}_v - \left[\sum_{i=1}^{2}(-1)^{i+1}k_i a_i\sin(\frac{\pi x_{ci}}{L})\right]q_b + (k_1a_1 - k_2a_2)z_v + (k_1a_1^2 + k_2a_2^2)\theta_v = 0 \tag{10}$$

Eqs. (8)–(10) can be arranged into the matrix format, as shown in Eq. (11),

$$\mathbf{M}_s[\ddot{q}_b, \ddot{z}_v, \ddot{\theta}_v]^T + \mathbf{K}_s\left[q_b, z_v, \theta_v\right]^T = \mathbf{f}_s \tag{11}$$

where $\mathbf{M}_s$, $\mathbf{K}_s$ are the mass and stiffness matrices of the VBI system, and the vector $\mathbf{f}_s$ are forces applied. Their entries are shown in Eqs. (12)–(14).

$$\mathbf{M}_s = \begin{bmatrix} \frac{\overline{m}L}{2} & 0 & 0 \\ 0 & m_v & 0 \\ 0 & 0 & J_v \end{bmatrix} \tag{12}$$

$$\mathbf{K}_s = \begin{bmatrix} \frac{EI\pi^4}{2L^3} + \sum_{i=1}^{2}k_i\sin^2(\frac{\pi x_{ci}}{L}) & -\sum_{i=1}^{2}k_i\sin(\frac{\pi x_{ci}}{L}) & -\sum_{i=1}^{2}(-1)^{i+1}k_i a_i\sin(\frac{\pi x_{ci}}{L}) \\ -\sum_{i=1}^{2}k_i\sin(\frac{\pi x_{ci}}{L}) & k_1 + k_2 & k_1a_1 - k_2a_2 \\ -\sum_{i=1}^{2}(-1)^{i+1}k_i a_i\sin(\frac{\pi x_{ci}}{L}) & k_1a_1 - k_2a_2 & k_1a_1^2 + k_2a_2^2 \end{bmatrix} \tag{13}$$

$$\mathbf{f}_s = \left[-\sum_{i=1}^{2}m_{vi}g\sin(\frac{\pi x_{ci}}{L}), 0, 0\right]^T \tag{14}$$

The equations provided above factor in the interaction between the two-axle vehicle and bridge. It is noteworthy that the stiffness matrix of the VBI system exhibits a temporal change as the vehicle passes the bridge. Consequently, the frequencies of both the bridge and the vehicle will undergo variations. When the two systems, i.e. the vehicle and bridge, are considered independently without interaction, they have their original frequencies, respectively. For the bridge, its original fundamental frequency can be calculated by Eq. (15).

$$\omega_{b1,0} = \frac{\pi^2}{L^2}\sqrt{\frac{EI}{\overline{m}}} \tag{15}$$

For the vehicle, the vertical and pitching frequencies of the two-axle vehicle can be obtained by solving the generalized eigenvalue problems of its mass and stiffness matrices. The solutions related to the original frequencies of the vehicle have been investigated by the Ref. [37], as shown in Eq. (16).

$$\omega_{v0,p0}^2 = \frac{1}{2}\left(\frac{k_1 + k_2}{m_v} + \frac{k_1a_1^2 + k_2a_2^2}{J_v} \pm \sqrt{\left(\frac{k_1 + k_2}{m_v} - \frac{k_1a_1^2 + k_2a_2^2}{J_v}\right)^2 + \frac{4\left(k_1a_1 - k_2a_2\right)^2}{m_vJ_v}}\right) \tag{16}$$

Here, $\omega_{v0,p0}$ represents the original frequencies of the vehicle without interaction with the bridge. During the interaction process between the vehicle and bridge, time-varying frequencies of the system can be obtained by solving the eigenvalue problem, as shown in Eq. (17).

$$\det(\mathbf{K}_s - \omega^2\mathbf{M}_s) = 0 \tag{17}$$

Set $\Omega = \omega^2, \Omega > 0$, and it can be noticed that Eq. (17) is a cubic equation with regard to Ω. Even though it can be analytically solved by Cardano's formula [38], the analytical solution will become extremely complex and meaningless for this problem. A practical way to solve Eq. (17) is to seek for numerical roots when the values of other parameters are known except Ω. As $\mathbf{K}_s$ and $\mathbf{M}_s$ include only real numbers and are symmetrical and positive definite, Ω can always be obtained as real and positive. Then, the time-varying frequencies of the VBI system, i.e. ω_{b1}, ω_v, and ω_p, can be obtained by $\omega = \sqrt{\Omega}$ when the vehicle is on different positions of the bridge.

2.2. Time-varying frequency identification using IMSST and ridge extraction

While the above model provides semi-analytical solutions, it is typically challenging to accurately capture the time-varying frequencies of the VBI system in practice due to the Heisenberg uncertainty principle of conventional time–frequency analysis methods such as STFT and wavelet transform. The TFRs generated by these methods are often too blurry to accurately extract the time-varying features of signals. This paper explores the potential of the IMSST to identify frequency variations within the VBI system. The non-stationary signal $s(t)$ of the two-axle vehicle within the VBI system can be represented by Eq. (18),

$$s(t) = A(t)\mathrm{e}^{\mathrm{i}\phi(t)} \tag{18}$$

where $A(t)$ denotes the instantaneous amplitude, while $\phi(t)$ is the instantaneous phase. For non-stationary signals, the fast Fourier transform (FFT) is unable to capture their time-varying characteristics effectively. To address this issue, the STFT was proposed, which utilizes sequential windows and FFT. Let the window function be denoted as $g(t)$ and its complex conjugate as $g^*(t)$. Assuming that the signal is weakly time-varying, according to the Auger et al. [39], we can get the STFT of the signal $s(\tau)$ using Eq. (19),

$$G(t,\omega) = \int_{\mathbb{R}} g^*(\tau - t)s(\tau)\mathrm{e}^{-\mathrm{i}\omega\tau}d\tau = A(t)\mathrm{e}^{\mathrm{i}\phi(t)}\hat{g}\left(\omega - \phi'(t)\right) \tag{19}$$

where $\hat{g}(\cdot)$ means the Fourier transform of the window function $g(\cdot)$. From Eq. (19), we can see that with the introduction of time t and window functions, the signal representation is now in a 2-dimensional TF plane. However, because the TF atoms are restricted by the Heisenberg uncertainty principle, the STFT only offers a blurry description of the signal. The SST utilizes a frequency-reassignment operator to collect spread TF coefficients, allowing for a more precise representation, which can be represented as

$$Ts^{[0]}(t,\eta) = \int_{\mathbb{R}} G(t,\omega)\delta(\eta - \hat{\omega}(t,\omega))d\omega \tag{20}$$

where $\delta(\cdot)$ represents the Dirac delta function, which is the same as in Eq. (1). The 2-dimensional estimation for the STFT results is denoted by $\hat{\omega}(t,\omega)$. While SST may not be quite proficient in handling strong frequency-modulated signals, the frequencies of the vehicle and bridge are relatively stable and tend to change smoothly. Hence, SST can be a suitable candidate for identifying their time-varying features. Moreover, by using SST once, the original blurry TFRs of STFT will be sharpened once. The updated TFR can be better than the original one. Thus, it is instinctive to employ SST multiple times to further sharpen the obtained TFRs. By employing SST iteratively for K times, we can get the representation of MSST [40], as shown in Eq. (21), where K means the number of total iterations before getting the final TFR.

$$Ts^{[k]}(t,\eta) = \int_{\mathbb{R}} Ts^{[k-1]}(t,\omega)\delta(\eta - \hat{\omega}(t,\omega))d\omega, k = 1,2,3,\ldots,K. \tag{21}$$

Notwithstanding, it was found that employing SST several times requires much computational resources. The above equation can be solved by the following two steps: (1) construct a new IF estimation $\hat{\omega}^{[K]}(t,\omega)$, and then (2) the SST is executed only once, as shown in Eq. (22),

$$Ts^{[K]}(t,\eta) = \int_{\mathbb{R}} G(t,\omega)\delta\left(\eta - \hat{\omega}^{[K]}(t,\omega)\right)\mathrm{d}\omega \tag{22}$$

where $\hat{\omega}^{[K]}(t,\omega)$ represents that $\hat{\omega}(t,\omega)$ is executed K times, and for each time, the newly obtained $\hat{\omega}$ is used as ω in the next time. However, during the application of the MSST, it was observed that for certain signals, increasing the iterations of using SST can still be influenced by the issue of non-reassigned points. This, in turn, can lead to blurry energy problems at certain points in the TF domain. It was discovered that this problem arises due to the rounding operation in two consecutive iterations. In 2021, Yu proposed a solution to address this blurry energy problem in the MSST [36]. The main modification is that before the next iteration for obtaining $\hat{\omega}^{[k+1]}(t,\omega)$, in the kth iteration, the one-round process is replaced by Eq. (23), where R means the round process. The above-proposed method was then named as IMSST.

$$\hat{\omega}_{\mathrm{R}}^{[k]}(t,\omega) = \mathrm{R}\left(\mathrm{R}\left(2\hat{\omega}^{[k]}(t,\omega)\right)/2\right) \tag{23}$$

In practice, when the vehicle passes the bridge, the dynamic information of the bridge can be transferred to the vehicle due to their interaction, which makes the identification of bridge frequencies from vehicle responses possible. Likewise, during this interaction, the vehicle's dynamic characteristics will also be included in the bridge's vibrations. Thus, no matter the vehicle or bridge, their vibrations are multi-component signals, including the dynamic information of the VBI system. For the acceleration of the vehicle or bridge, it can be written as

$$s_{vbi}(t) = \sum_{j=1}^{N} s_{vbi,j}(t) = \sum_{j=1}^{N} A_j(t)\mathrm{e}^{\mathrm{i}\phi_j(t)} \tag{24}$$

where $s_{vbi,j}(t)$ is the jth component of the VBI system's responses; $\phi_j(t)$ means its instantaneous phase. The instantaneous frequency value can be obtained by its first-order derivative $\phi_j'(t)$. Assuming that each component can be separated by a certain distance, the STFT of the multi-component signal can be approximated by the summation of the first-order Taylor expansion of each component [41], as shown in Eq. (25). Then, by substituting Eq. (25) into Eqs. (20)–(23), we can get TFRs of the multi-component signal.

$$G(\omega,t) = \sum_{j=1}^{N} G_j(\omega,t) \approx \sum_{j=1}^{N} A_j(t)\mathrm{e}^{\mathrm{i}\phi_j(t)}\hat{g}\left(\omega - \phi_j'(t)\right) \tag{25}$$

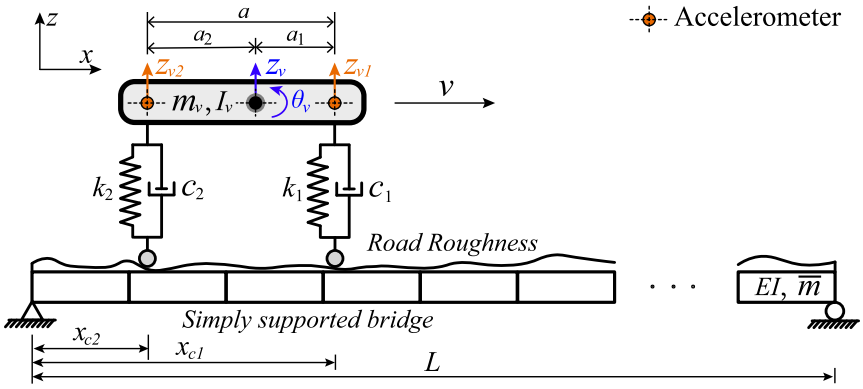

Fig. 2. Numerical model of the two-axle vehicle and bridge.

After the IMSST is employed, the energy of TFR can be more concentrated, thus the time-varying frequency values can be easily extracted. In this paper, a popular multi-ridge extraction algorithm is employed, which relies on minimizing Eq. (26) [42,43]. Here, $\varphi_j(t)$ is the estimation of $\phi_j'(t)$; N is the number of modes that we have to determine before seeking for IF trajectories; λ_1 and λ_2 are regularization parameters that maximize the trade-off between smoothness of $\varphi_j(t)$ and the kept energy.

$$E(\varphi) = \sum_{j=1}^{N} - \int_{\mathbb{R}} \left| \mathrm{TFR}\left(t, \varphi_j(t)\right) \right|^2 dt + \int_{\mathbb{R}} \lambda_1 \varphi_j'(t)^2 + \lambda_2 \varphi_j''(t)^2 dt \tag{26}$$

3. Numerical simulations

The previous section introduced semi-analytical solutions for the time-varying frequencies of the VBI system. Deriving (semi-)analytical solutions for vehicle responses typically requires some assumptions, such as $m_v \ll \overline{m}L$ [10]. Also, including more parameters in the derivation will make it quite complex or impossible to achieve, e.g., the consideration of bridge damping [12,22]. In the following sections, significant conditions such as the inclusion of vehicle damping, bridge damping, and road roughness will be explored in the VBI process. These conditions will significantly increase the complexity of deriving analytical solutions for vehicle responses. Therefore, it is necessary to perform finite element (FE) modeling, which has simple concepts and is easy to conduct. Moreover, the results of FE modeling can be used to verify the previously derived semi-analytical solutions. For comparisons with the derivation of semi-analytical solutions, the 2-dimensional (2D) FE modeling approach is adopted here. Compared to 3-dimensional (3D) modeling, 2D modeling is widely employed and reliable in achieving relatively good accuracy but requires fewer computational resources [44]. The verification of semi-analytical solutions via these simulations is the initial step, followed by showcasing the efficiency of IMSST in identifying time-varying frequencies of the system. Subsequently, based on the semi-analytical solutions, the frequency amplification ratios with different parameters of vehicles will be investigated. Afterward, an analysis of several influencing factors in engineering will be provided.

3.1. FE model of the VBI system

The FE model of the two-axle vehicle and bridge can be found in Fig. 2. According to the Ref. [37], the equilibrium equations for the system are shown in Eq. (27),

$$\mathbf{M}_s^N[\ddot{\mathbf{z}}_b, \ddot{z}_v, \ddot{\theta}_v]^T + \mathbf{C}_s^N[\dot{\mathbf{z}}_b, \dot{z}_v, \dot{\theta}_v]^T + \mathbf{K}_s^N\left[\mathbf{z}_b, z_v, \theta_v\right]^T = \mathbf{f}_s^N \tag{27}$$

where $\boldsymbol{z}_b$ represents the vibrations of the bridge, z_v denotes the vertical displacement of the vehicle, and θ_v represents the rotation of the vehicle. Suppose that the bridge has n DOFs. Then, the mass and stiffness matrices of the VBI system can be represented by $\mathbf{M}_s^N$ and $\mathbf{K}_s^N$ including $(n+2)\times(n+2)$ entries. Here, N in the top right corner represents numerical simulations. The equations for the mass, damping, and stiffness matrices used in the simulations can be found in Eqs. (28)–(34) [37],

$$\mathbf{M}_s^N = \begin{bmatrix} \mathbf{M}_b & 0_{n\times 1} & 0_{n\times 1} \\ 0_{1\times n} & m_v & 0 \\ 0_{1\times n} & 0 & J_v \end{bmatrix} \tag{28}$$

$$\mathbf{C}_s^N = \begin{bmatrix} \mathbf{C}_b + \left(c_2\mathbf{n}_2^T\mathbf{n}_2 + c_1\mathbf{n}_1^T\mathbf{n}_1\right) & -\left(c_2\mathbf{n}_2^T + c_1\mathbf{n}_1^T\right) & c_2a_2\mathbf{n}_2^T - c_1a_1\mathbf{n}_1^T \\ -c_2\mathbf{n}_2 - c_1\mathbf{n}_1 & c_1 + c_2 & c_1a_1 - c_2a_2 \\ c_2\mathbf{n}_2a_2 - c_1\mathbf{n}_1a_1 & c_1a_1 - c_2a_2 & c_1a_1^2 + c_2a_2^2 \end{bmatrix} \tag{29}$$

$$\mathbf{K}_s^N = \begin{bmatrix} \mathbf{K}_b + \boldsymbol{\Lambda}_{11} & -\left(k_2\mathbf{n}_2^T + k_1\mathbf{n}_1^T\right) & k_2a_2\mathbf{n}_2^T - k_1a_1\mathbf{n}_1^T \\ \boldsymbol{\kappa}_{21} & k_1 + k_2 & k_1a_1 - k_2a_2 \\ \boldsymbol{\kappa}_{31} & k_1a_1 - k_2a_2 & k_1a_1^2 + k_2a_2^2 \end{bmatrix} \tag{30}$$

Table 1
Vehicles with different parameters.

Vehicle No.	$k_1 = k_2$ (kN)	f_v^0 (Hz)	f_p^0 (Hz)	f_v^0/f_{b1}^0	f_p^0/f_{b1}^0	Note
1	90	1.758	3.100	0.487	0.859	–
2	120	2.030	3.580	0.562	0.992	Near resonance
3	124	2.063	3.639	0.572	1.008	Near resonance
4	250	2.930	5.167	0.812	1.432	–
5	370	3.564	6.286	0.987	1.742	Near resonance
6	390	3.659	6.454	1.014	1.788	Near resonance
7	600	4.539	8.005	1.257	2.218	–
8	6.0×10^8	4539	8005	1257	2218	Moving mass
9	0.6×10^{-3}	0.005	0.008	0.001	0.002	Moving load

$$\mathbf{\Lambda}_{11} = k_2\mathbf{n}_2^T\mathbf{n}_2 + c_2 v\mathbf{n}_2^T\mathbf{n}_2' + k_1\mathbf{n}_1^T\mathbf{n}_1 + c_1 v\mathbf{n}_1^T\mathbf{n}_1' \tag{31}$$

$$\boldsymbol{\kappa}_{21} = -k_2\mathbf{n}_2 - c_2 v\mathbf{n}_2' - k_1\mathbf{n}_1 - c_1 v\mathbf{n}_1' \tag{32}$$

$$\boldsymbol{\kappa}_{31} = a_2 c_2 v\mathbf{n}_2' + a_2 k_2\mathbf{n}_2 - a_1 k_1\mathbf{n}_1 - a_1 c_1 v\mathbf{n}_1' \tag{33}$$

$$\mathbf{f}_s^N = -\begin{bmatrix} \left(m_v g a_1/a - k_2 z_{r2} - c_2 v z_{r2}'\right)\mathbf{n}_2^T + \left(m_v g a_2/a - k_1 z_{r1} - c_1 v z_{r1}'\right)\mathbf{n}_1^T \\ k_2 z_{r2} + c_2 v z_{r2}' + k_1 z_{r1} + c_1 v z_{r1}' \\ -a_2 c_2 v z_{r2}' - a_2 k_2 z_{r2} + a_1 k_1 z_{r1} + a_1 c_1 v z_{r1}' \end{bmatrix} \tag{34}$$

where $\mathbf{M}_b$, $\mathbf{C}_b$, and $\mathbf{K}_b$ are the mass, damping, and stiffness matrices of the bridge. $\mathbf{n}_i$ is the force distribution vector that can be represented by $\mathbf{n}_i = [0, \ldots, \mathbf{h}_i, \ldots, 0], i = 1, 2$. Here, $\mathbf{h}_i$ denotes the Hermitian interpolation function that calculates the coefficients for force distribution when the vehicle's axle is not located on the nodes of the bridge [14]. The variable z_{ri} represents the road roughness under the ith contact point between the vehicle and bridge. All other parameters have the same definitions as the semi-analytical solution discussed in Section 2.1.

3.2. Verification of semi-analytical solutions and IMSST

The parameters of the VBI system used in this section are taken from the Ref. [45], and we consider nine vehicles with varying suspension stiffness. Here, the commonly used assumption that front and rear suspensions share the same stiffness values is adopted [12,37,45]. Then, the frequencies of the vehicle can be easily adjusted by changing the value $k_1 = k_2$. It is worth noting that findings in this work are not limited to such assumption, but it is merely for the simplification of modifying the vehicle's frequencies. For vehicles 2, 3, 5, and 6, one of the vehicles' frequencies is close to the fundamental frequency of the bridge. On the other hand, vehicles 1, 4, and 7 represent common cases where there is no resonance with the bridge. To simulate a moving mass or load, the suspension stiffness for vehicles 8 and 9 is significantly increased or decreased, respectively [33]. In the following analysis, the frequency (f) expressed in Hz is utilized instead of the circular frequency (ω) in rad/s. Here, $f_{b1}^0 = \omega_{b1,0}/2\pi$, and $f_{v,p}^0 = \omega_{v0,p0}/2\pi$. The shared parameters for all vehicles are as follows: $m_v = 1000$ kg, $J_v = 700$ kg $\cdot$ m^2, $a_1 = 0.5$ m, $a_2 = 1.5$ m. The utilized parameters for vehicle suspensions are listed in Table 1. The stiffness values k_1 and k_2 are primarily utilized to adjust the vertical and pitching frequencies of the two-axle vehicle to make them smaller than, slightly smaller than, slightly greater than, and greater than the bridge's frequency. There are in total 7 scenarios as shown in Table 1 (Vehicles 1–7). In engineering, any of these 7 scenarios can occur due to the difference between vehicle frequencies and bridge frequencies. Specifically, for vehicle 1, its vertical and pitching frequencies are both lower than the bridge's fundamental frequency f_{b1}^0. In contrast, vehicles 2 and 3 have pitching frequencies nearly resonant with the bridge, although their vertical frequencies are significantly below f_{b1}^0. Vehicle 4's pitching frequency exceeds f_{b1}^0, while its vertical frequency remains below the bridge's fundamental frequency. Vehicle 5 has a slightly lower vertical frequency while vehicle 6 has a slightly higher vertical frequency than f_{b1}^0, which could also potentially lead to resonance. Vehicle 7 represents the scenario when both its vertical and pitching frequencies have greatly exceeded the bridge's fundamental frequency. Lastly, vehicles 8 and 9 simulate the cases of moving mass and moving load, characterized by extremely high and low vehicle stiffness, respectively.

To track the time-varying frequencies of the VBI system using IMSST, the vehicle's responses are collected by two unidirectional accelerometers (shown in Fig. 2) attached to the vehicle, and the vehicle's vertical and angular accelerations ($\ddot{z}_v, \ddot{\theta}_v$) can be calculated by Eq. (35). The vehicle's speed is set to 2 m/s.

$$\ddot{z}_v = (\ddot{z}_{v1}a_2 + \ddot{z}_{v2}a_1)/a, \ddot{\theta}_v = (\ddot{z}_{v1} - \ddot{z}_{v2})/a \tag{35}$$

The bridge is divided into 50 elements, with the following parameters: $L = 25$ m, $E = 27.5$ GPa, $I = 0.15$ m^4, and $\overline{m} = 2000$ kg/m. With these parameters, the original frequencies of the bridge without interaction with vehicles can be calculated as $f_{b1}^0 = 3.609$ Hz, $f_{b2}^0 = 14.438$ Hz, $f_{b3}^0 = 32.485$ Hz. Damping effects and road roughness are temporarily ignored for theoretical validations in this section.

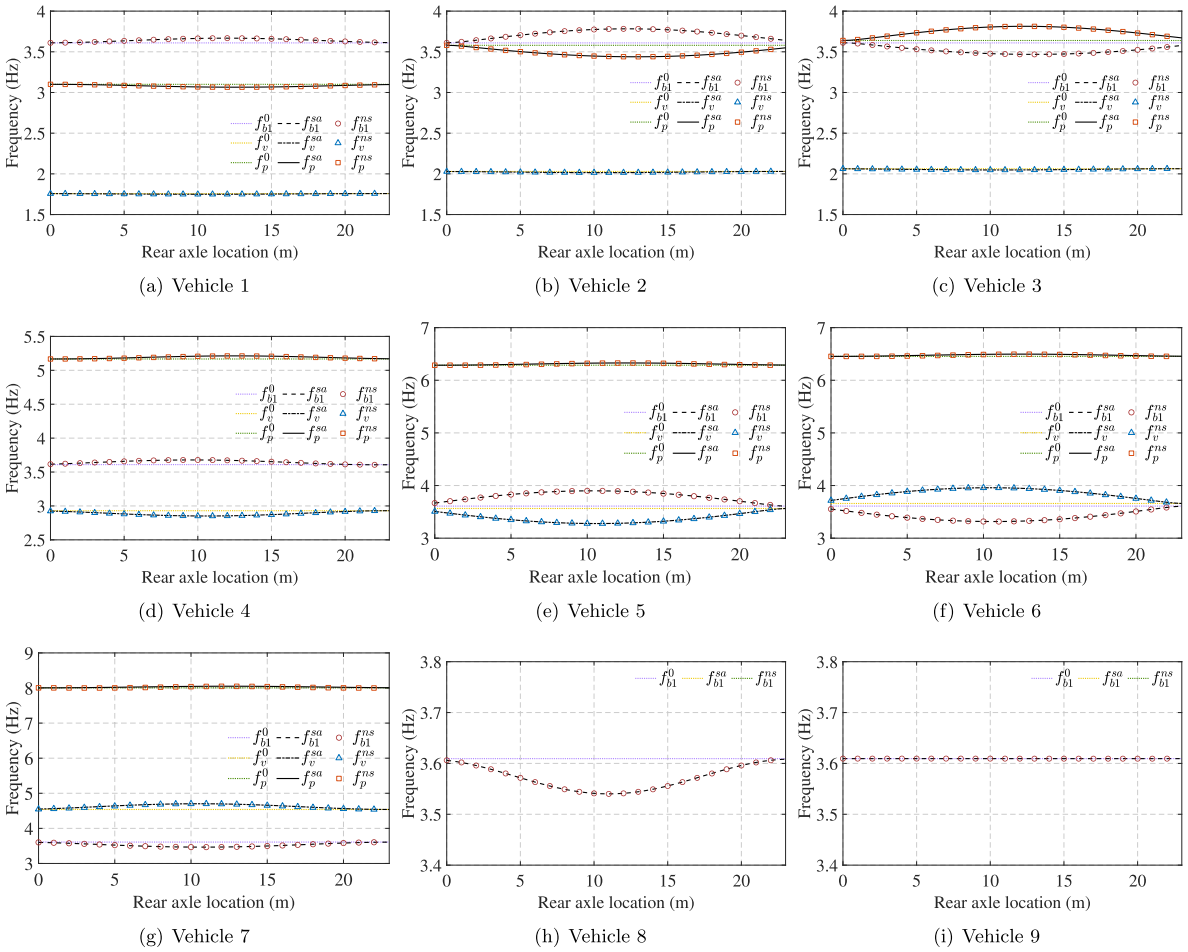

Fig. 3. Frequency variation of the VBI system with different vehicles.

The frequencies of the VBI system in numerical simulations have been plotted in Fig. 3, along with the frequencies obtained from semi-analytical solutions derived in Section 2.1. It is evident that the semi-analytical solutions closely align with the numerical results for all vehicles. Hence, the theory developed for determining the varying frequencies of the VBI system can be deemed reliable.

Additionally, Fig. 3 illustrates that when both frequencies of the vehicle are smaller than f_{b1}^0 (vehicle 1), both vehicle frequencies decrease as they traverse the bridge, while the bridge's frequency increases during this passage. When the vertical and pitching frequencies of the vehicle are on opposite sides of the bridge's fundamental frequency (vehicle 4), it can be observed that the pitching frequency of the vehicle increases while the vertical frequency decreases when on the bridge. Simultaneously, the bridge's fundamental frequency also experiences an increase. Conversely, when the frequencies of the vehicle surpass the first mode of the bridge (vehicle 7), the bridge's fundamental frequency decreases during the passage, while the vehicle frequencies increase.

Furthermore, it is clear that the frequency variation amplitudes of vehicles 1, 4, and 7 are relatively low during their passages. However, when a possible resonance occurs between the vehicle and bridge, frequency variations become more pronounced, as observed with vehicles 2, 3, 5, and 6. In addition, it can be observed that when the frequencies of the vehicles are slightly lower than f_{b1}^0 (vehicles 2 and 5), the bridge's fundamental frequency increases during the passage, while the frequency of the vehicles, which is close f_{b1}^0, decrease significantly. Conversely, when the frequencies of the vehicles are slightly higher than f_{b1}^0 (vehicles 3 and 6), the bridge's fundamental frequency experiences a substantial decrease, and the vehicle's frequency near f_{b1}^0 increases sharply.

For vehicles 8 and 9 (representing the moving mass and force), their frequencies are meaningless and therefore are not plotted in Fig. 3. It is evident that when the vehicle mass passes the bridge, the bridge's fundamental frequency decreases significantly, aligning with the findings in Ref. [33]. However, when the vehicle is regarded as a moving force, the fundamental frequency of the bridge remains unchanged and equals f_{b1}^0 during the passage.

In engineering applications, TFA tools need to be used to track the variation of frequencies of a signal. In this study, the IMSST method is utilized to capture the system's time-varying frequencies. Vehicle 7 is employed to verify the effectiveness of IMSST. Fig. 4 presents the results of frequency extraction using the vehicle's vertical accelerations, with a window length of 5200. From

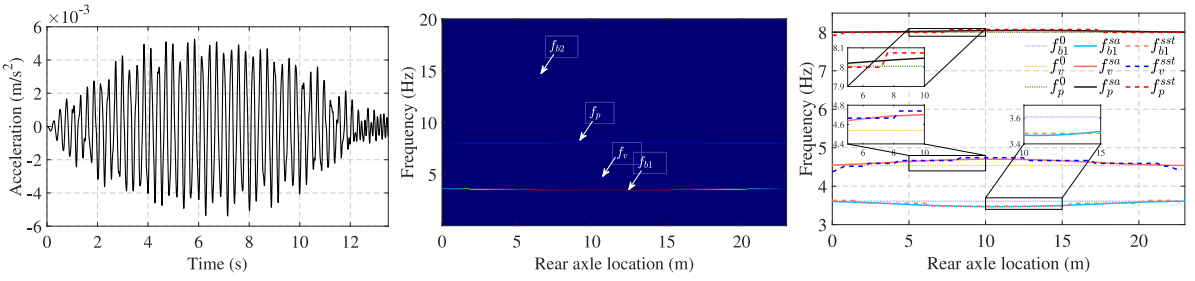

(a) Vehicle's vertical accelerations (b) TFRs using IMSST (c) Ridge extraction

Fig. 4. Verification of frequency extraction using IMSST and the vehicle's vertical accelerations.

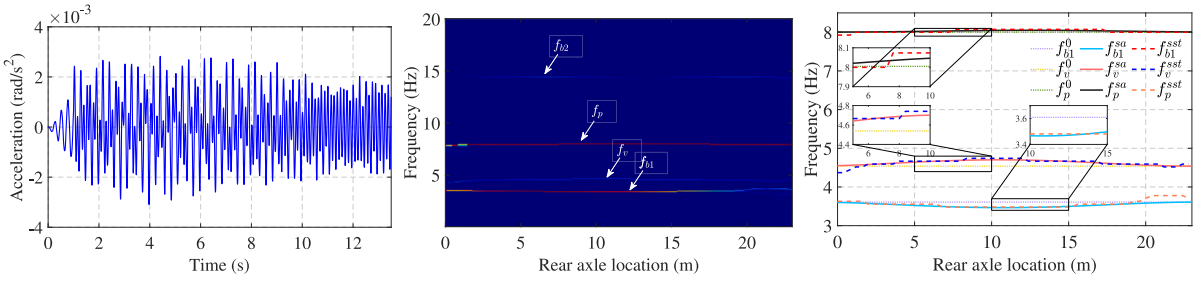

(a) Vehicle's rotational accelerations (b) TFRs using IMSST (c) Ridge extraction

Fig. 5. Verification of frequency extraction using IMSST and the vehicle's rotational accelerations.

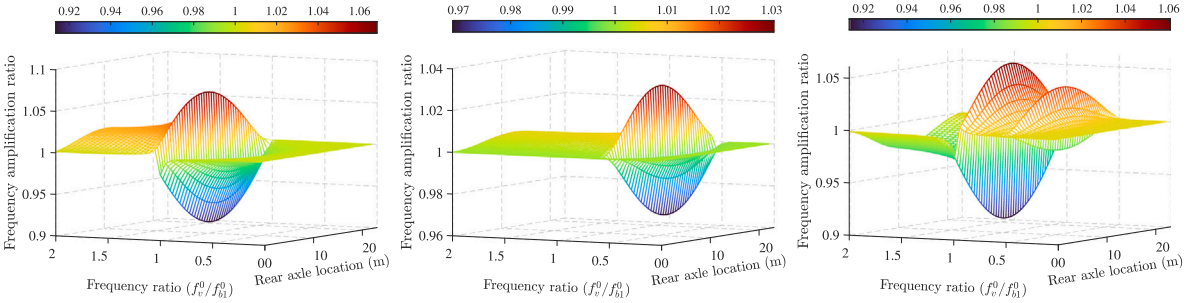

(a) Variation of f_v (b) Variation of f_p (c) Variation of f_{b1}

Fig. 6. VBI system's frequency amplification with respect to vehicle–bridge frequency ratio.

Fig. 4b, it can be observed that the IMSST method successfully identifies the vehicle's vertical and pitching frequencies, as well as the bridge's first two frequencies, along with their variations during the interaction. From Fig. 4c, one can see that the variation of the VBI system has been roughly captured after the ridge extraction technique is employed. The identified frequency changes can track the theoretical values well.

Similarly, Fig. 5 illustrates the results of time-varying frequency extraction using the vehicle's rotational accelerations. Fig. 5b clearly shows that the variation of the vehicle's pitching frequency can be better identified compared to the frequency change tracks in Fig. 4b. Additionally, Fig. 5c demonstrates that the variations of the VBI system's frequencies can also be identified. Therefore, by examining Figs. 4 and 5, it is evident that the proposed IMSST-based frequency variation identification method can successfully identify the VBI system's time-varying frequencies using either the vehicle's vertical or pitching accelerations.

3.3. Frequency amplification ratio analysis

Upon analysis in the aforementioned paragraphs, it becomes apparent that the frequencies of the VBI system can vary, either increasing or decreasing, depending on the characteristics of the vehicle. To further explore this variation, we examined the frequency variation amplification ratio of the system with respect to the vehicle–bridge frequency ratio (f_v^0/f_{b1}^0) and mass ratio ($m_v/\overline{m}L$), as illustrated in Figs. 6 and 7. The subsequent analysis is based on the parameters of vehicle 7 in Table 1.

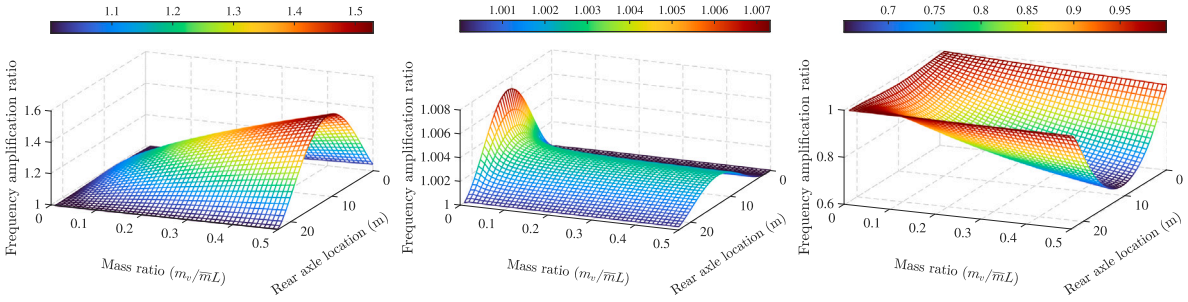

(a) Variation of f_v (b) Variation of f_p (c) Variation of f_{b1}

Fig. 7. VBI system's frequency amplification with respect to vehicle–bridge mass ratio.

When analyzing the frequency ratio, the mass ratio between the vehicle and bridge is kept fixed at 1000/2000/25 = 0.02. The frequency ratio f_v^0/f_{b1}^0 is then varied from 0.05 to 2, with an interval of 0.05. The results of this analysis are presented in Fig. 6.

Firstly, for the vertical frequency of the vehicle, f_v, the analysis of Fig. 6a reveals that the largest variation in the amplification ratio f_v/f_v^0 occurs when resonance occurs, that is, when f_v^0 is nearly equal to f_{b1}^0. Specifically, when the frequency ratio is slightly greater than 1.0, the vehicle's vertical frequency increases as it passes through the bridge, reaching its maximum at the midpoint of the bridge. Conversely, when the frequency ratio is slightly smaller than 1.0, f_v sharply decreases as the vehicle passes through the bridge, with the minimum amplification reached at the midpoint of the bridge.

Furthermore, for the pitching frequency of the vehicle, f_p, similar effects can be observed as shown in Fig. 6b. However, the maximum amplification ratio occurs when the frequency ratio (f_v^0/f_{b1}^0) is approximately 0.6. Upon further observation by the authors, it is determined that this is the moment when resonance occurs between the first frequency of the bridge (f_{b1}^0) and the pitching frequency of the vehicle (f_p^0). This implies that the vehicle's pitching frequency is also influenced by the fundamental frequency of the bridge. Furthermore, it can be noted that the maximum amplification value of f_p (1.03) is slightly smaller than that of f_v (1.05).

Thirdly, Fig. 6c illustrates amplification ratios of the bridge's fundamental frequency, f_{b1}. We can see that there are two peaks on the Y-axis (frequency ratio). These peaks occur when the resonance between the bridge's fundamental frequency and the vehicle's vertical or pitching frequencies takes place. Additionally, it can be observed that the amplification ratio is greater when the resonance occurs between f_v^0 and f_{b1}^0 compared to when it occurs between f_p^0 and f_{b1}^0. Unlike the vehicle's frequencies, when the frequency ratio is slightly smaller than 1.0, f_{b1} decreases, whereas it increases when the frequency ratio is slightly greater than 1.0. A similar phenomenon can be observed when the vehicle's pitching frequency is close to the bridge's fundamental frequency. Therefore, it is apparent that in analyzing the interaction between the vehicle and bridge, it is necessary to consider not only the vehicle's vertical frequency but also additional vehicular frequencies, such as the pitching frequency.

The mass ratio between the vehicle and the bridge, denoted as $m_v/\overline{m}L$, is another significant factor to consider. To investigate the impact of this ratio on the time-varying characteristics of the VBI system's frequencies, we keep the ratio between the vehicle's vertical frequency (f_v^0) and the bridge's fundamental frequency (f_{b1}^0) constant at 1.257. The mass ratio is varied from 0.01 to 0.5, with increments of 0.01. The resulting time-varying frequencies of the VBI system are shown in Fig. 7.

From Fig. 7a, it can be observed that the vertical frequency f_v of the two-axle vehicle increases when it passes over the bridge. This increase is more pronounced with larger vehicle masses. When the mass ratio is 0.5, the frequency amplification ratio of the vehicle can exceed 1.5. The pitching frequency f_p of the vehicle, as shown in Fig. 7b, also increases when the vehicle crosses the bridge. However, the frequency amplification pattern of f_p is different from that of f_v. For lower mass ratios (e.g., 0.01–0.05), the frequency amplification ratio during the vehicle's passage varies more significantly and can exceed 1.007. As the mass ratio increases, the frequency amplification ratio becomes more stable and does not vary greatly. The variation of the bridge's fundamental frequency f_{b1} with different mass ratios is shown in Fig. 7c. It can be observed that f_{b1} decreases as the vehicle passes the bridge. This decrease becomes more significant with higher mass ratios. When the mass ratio is 0.5, the frequency amplification ratio can be lower than 0.65. Based on the above observations, we can draw the following conclusions: (1) The greatest variation in frequency occurs when the vehicle passes the midpoint of the bridge. (2) f_v and f_{b1} can be significantly affected by high vehicle–bridge mass ratios, while f_p is easily influenced by low vehicle–bridge mass ratios. Therefore, when analyzing VBI systems using passing vehicles as excitation sources, it is advisable to ensure that the mass of the vehicle is relatively small compared to that of the bridge. Based on the analysis, a mass ratio of 0.05 is recommended to minimize any significant impact on the frequencies of the VBI system. However, in practical applications, the focus is usually on the frequencies of the bridge. To maintain these frequencies relatively constant, it is necessary to keep the vehicle–bridge mass ratio as low as possible.

In practical engineering, the variations in the bridge's frequency are typically of interest to researchers. To investigate the influence of vehicle–bridge frequency and mass ratios on the fundamental frequency of the bridge, Fig. 8 is presented. This figure represents the maximum frequency amplification ratios of f_{b1}, specifically when the vehicle's center of gravity is passing the midpoint of the bridge. Two different X-axes are used to represent the amplification effects. Fig. 8a demonstrates that as the ratio f_v^0/f_{b1}^0 increases, frequency amplification peaks and valleys begin to emerge when it approaches 0.4. Comparing this with Fig. 8b, we can

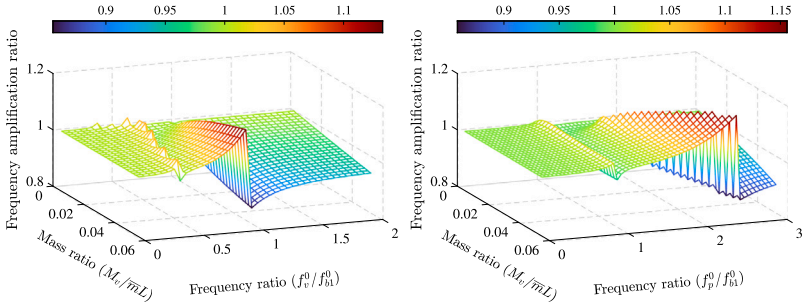

(a) X-axis: f_v^0/f_{b1}^0 (b) X-axis: f_p^0/f_{b1}^0

Fig. 8. Maximum frequency amplification of f_{b1} with respect to vehicle–bridge frequency and mass ratios.

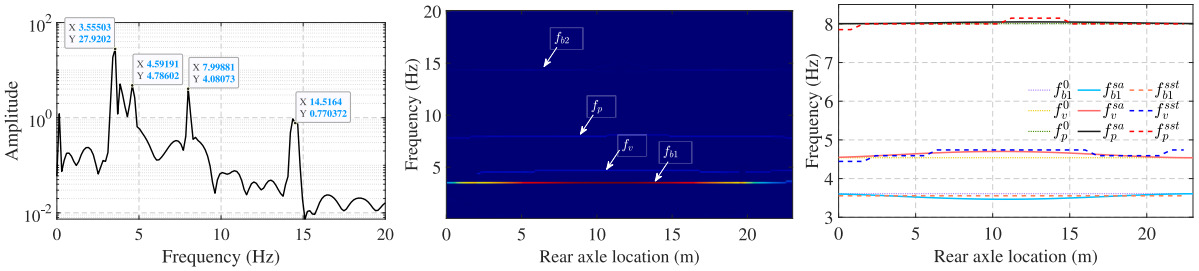

(a) FFT (b) TFRs using IMSST (c) Ridge extraction

Fig. 9. Frequency identification of the VBI system with a higher vehicle speed of 4 m/s.

observe that even though f_v^0/f_{b1}^0 is less than 1.0, f_p^0/f_{b1}^0 is already approaching 1.0, resulting in low-peak frequency amplifications. Furthermore, we can see that these low peaks and valleys are minimally affected by the mass ratios. As f_v^0/f_{b1}^0 increases in Fig. 8a, it becomes evident that when it is around 1.0, the highest peak and valley appear. Currently, We can see that the ratio f_p^0/f_{b1}^0 gradually increases from 1.5 to 2.5. Additionally, the mass ratio significantly influences the frequency amplification, and lower vehicle–bridge mass ratios have relatively limited effects. Therefore, based on the above analysis, it can be deduced that the resonance between the vehicle with a vertical frequency near f_{b1} has a greater impact on the bridge's fundamental frequency. However, the effects of the vehicle's pitching frequency can also cause non-negligible frequency variation amplification of f_{b1}, even if the mass ratio does not have a significant influence on the amplification.

3.4. Parametric analysis of the VBI system

The previous sections have discussed and analyzed the variations in frequencies of the VBI system as the vehicle passes through. However, there are several influential factors in engineering that can make it difficult to extract these time-varying frequencies. This section will discuss some common factors that can affect the extraction process, such as vehicle speed, vehicle damping, bridge damping, stiffness of the bridge and vehicle, environmental noise, and road roughness. To estimate the IFs of the system, the IMSST method is used. Unless otherwise stated, the parameters used for the VBI system are the same as those in Section 3.2.

3.4.1. Effect of vehicle speed

The speed of the vehicle is a crucial factor that affects the identification of the VBI system's IF. It primarily impacts the duration of the vehicle's passage, resulting in a lower frequency resolution in the frequency domain. Additionally, a lower vehicle speed causes weaker vibrations in the bridge. Conversely, higher speeds can lead to stronger vibrations induced by the vehicle, facilitating the transmission of bridge information to the passing vehicle. Hence, selecting an appropriate vehicle speed is important for extracting the VBI system's IFs. In this section, a higher speed of 4 m/s is considered, and Fig. 9 presents the frequency spectrum, TFRs using IMSST, and IF extraction results using the vehicle's vertical accelerations $\ddot{z}_v(t)$.

As shown in Fig. 9a, directly applying the FFT to the entire signal of the passing vehicle leads to invariant frequency values of the VBI system. To capture the time-varying features of the system, the IMSST is employed and the results of IF extraction are shown in Figs. 9b and c. Compared with Fig. 4c, we can see that the ability to capture frequency variation with respect to vehicle locations decreases. Specifically, for f_{b1}, the extracted IF becomes constant. For f_v and f_p, the extracted IFs do not closely align with the results of the semi-analytical approach. The primary reason behind this is that the increased speed results in a limited duration of the vehicle's acceleration, leading to shorter signals available for TFA. Consequently, maintaining the window length of IMSST makes it more challenging to capture frequency variation to vehicle locations. Similar findings have been reported in Refs. [22],

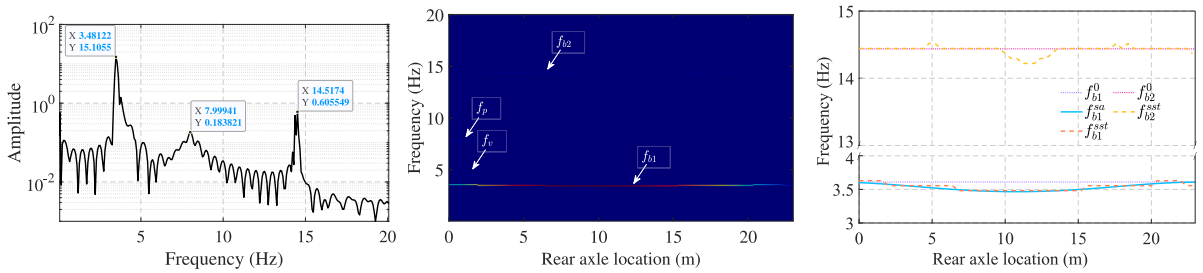

(a) FFT (b) TFRs using IMSST (c) Ridge extraction

Fig. 10. Frequency identification of the VBI system with vehicle damping of $c_1 = c_2 = 1$ kN·s/m.

where the vehicle's speed reaches 4 m/s, 15 m/s, or 20 m/s, resulting in less accessible variation of the VBI system's frequencies. Therefore, in practical engineering, when focusing on time-varying frequencies, it is recommended to keep the vehicle's speed low to obtain accurate TFRs of the VBI system.

3.4.2. *Effect of vehicle damping*

In the semi-analytical solutions, the damping of the vehicle is not taken into account. However, it is important to consider the damping of the vehicle as it may affect the transmission of the bridge's dynamic information to the moving two-axle vehicle. In engineering applications, the damping effects of suspension systems are typically present and cannot be eliminated through the design and manufacturing of test vehicles. In this section, the damping values for the vehicle's suspensions are set as $c_1 = c_2 = 1$ kN·s/m. The other parameters remain the same as in Section 3.2. The frequency spectrum, TFRs obtained through IMSST, and the extracted IFs are shown in Fig. 10.

From the results obtained using FFT, as shown in Fig. 10a, we can observe that the frequency f_v is completely imperceptible. Additionally, the peak of the vehicle's pitching frequency f_p is significantly lower compared to the bridge's frequencies, namely f_{b1} and f_{b2}. Fig. 10 suggests that f_p may be identifiable. However, when the TFRs of the vehicle's vertical accelerations are plotted, we notice that f_v and f_p only appear when the vehicle initially enters the bridge, and these traces quickly disappear due to the damping effects of the vehicle's suspension. The energy of the vehicle's pitching frequency only exists when the vehicle enters the bridge, and such a phenomenon is difficult to recognize by using merely FFT. Fig. 10c clearly demonstrates that the IFs of the bridge's time-varying fundamental frequency f_{b1} remain unaffected and can be accurately tracked during the vehicle's passage, while the second frequency is also observable. In the field of engineering, researchers typically focus on the bridge's frequencies, but in the frequency spectrum or TFRs, the vehicle's frequencies can always contaminate the extraction of bridge frequencies. Therefore, it is evident that utilizing vehicle suspension damping enables a clearer identification of bridge frequencies.

3.4.3. *Effect of bridge damping*

In this section, we utilize the Rayleigh damping assumption to model the bridge damping. The calculation of $\mathbf{C}_b$ can be performed using Eq. (36),

$$\mathbf{C}_b = \alpha \mathbf{M}_b + \beta \mathbf{K}_b \tag{36}$$

where $\mathbf{M}_b$, $\mathbf{C}_b$, and $\mathbf{K}_b$ are mass, damping, and stiffness matrices of the bridge, as introduced in Section 3.1. Normally, one could assume the same damping ratios for the bridge's first two modes, namely $\xi_1 = \xi_2 = \xi$. Then α and β could be calculated by Eq. (37),

$$[\alpha, \beta]^T = 2\xi/(w_{b1,0} + w_{b2,0})[w_{b1,0} \cdot w_{b2,0}, 1]^T \tag{37}$$

where $w_{b1,0}$ and $w_{b2,0}$ are the first two frequencies of the bridge without the vehicle on. In this section, we employ $\xi_1 = \xi_2 = 0.02$, which is commonly used in existing studies [13,46]. The identification results of the time-varying frequencies of the VBI system are presented in Fig. 11. Fig. 11a shows the frequency spectrum obtained from the vehicle's entire accelerations during its passage. Despite the absence of time-varying characteristics, the frequencies of the vehicle and the bridge's fundamental frequency can still be observed. However, the bridge's second frequency f_{b2} has noticeably decayed. Fig. 11b displays the TFRs of the vehicle's vertical accelerations. In the beginning, when the vehicle enters the bridge, f_{b1} and its variations are clearly identifiable. However, after the vehicle has traveled approximately 15 m, the trace for f_{b1} becomes fuzzy and cannot be accurately identified. This indicates that the bridge's damping has taken effect, weakening the vibrations transferred from the bridge to the vehicle. Nevertheless, the vehicle's dynamic information remains strong and identifiable. Fig. 11c shows the extracted IFs using ridge extraction. It can be observed that towards the end of the f_{b1} identification, the results become inaccurate and messy, failing to capture the variation of f_{b1}. Therefore, it is evident that the bridge's damping weakens the vibrations of the bridge, resulting in reduced information transmission to the vehicle and negatively impacting the identification of the bridge's IFs from the vehicle's responses.

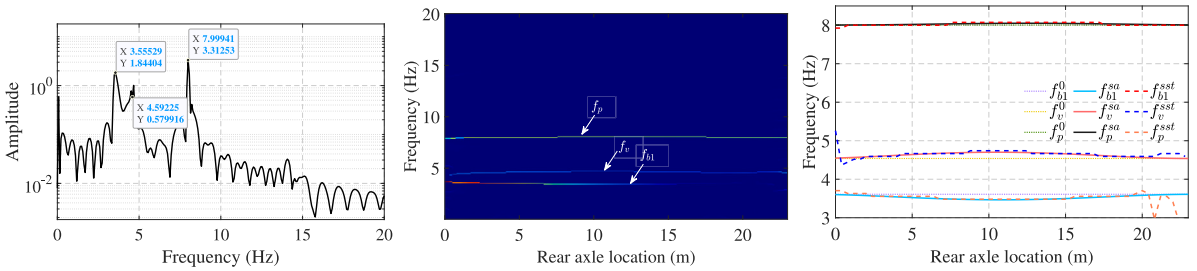

(a) FFT (b) TFRs using IMSST (c) Ridge extraction

Fig. 11. Frequency identification of the VBI system with bridge damping of $\xi_1 = \xi_2 = 0.02$.

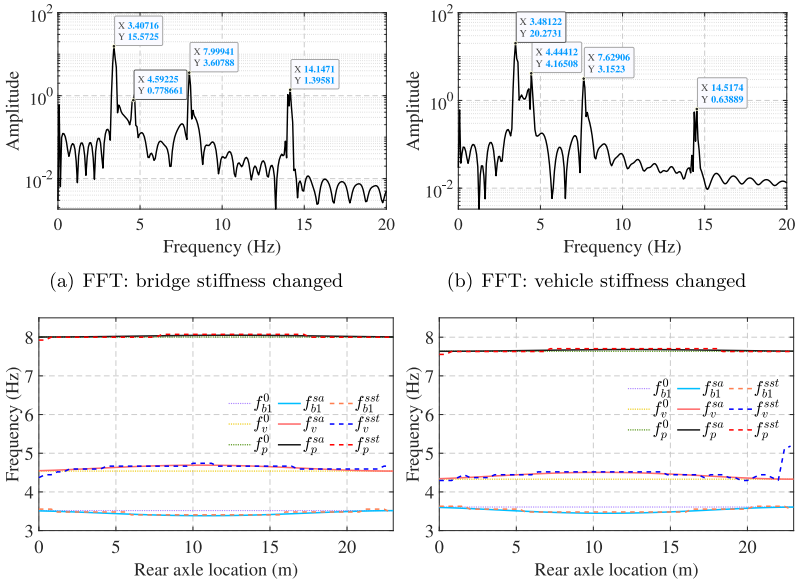

(a) FFT: bridge stiffness changed (b) FFT: vehicle stiffness changed

(c) Ridge extraction: bridge stiffness changed (d) Ridge extraction: vehicle stiffness changed

Fig. 12. Frequency identification of the VBI system using vehicle accelerations with changed stiffness of the bridge and vehicle.

3.4.4. Effect of stiffness of the bridge and vehicle

The stiffness of both the bridge and the vehicle is crucial in determining the frequencies of the VBI system and thus warrants further investigation when the IMSST is used to identify time-varying frequencies. In this section, we will discuss two scenarios: changes in the bridge's global flexural stiffness (EI) and changes in the vehicle's suspension stiffness (k_1 and k_2).

Due to deterioration and lack of maintenance, the bridge's global flexural stiffness can decrease [17]. In this study, a 5% loss in the bridge's global flexural stiffness is considered, represented as $E'I' = 0.95EI$ [47], while its mass remains unchanged. Under this condition, the bridge's original frequency decreases to $f_{b1}^{0\prime} = 3.518$ Hz. The indirect frequency identification results using FFT and extracted IFs from TFRs generated by IMSST are shown in Figs. 12a and c. We can see that the decrease in the bridge's fundamental frequency can also be detected by FFT when compared to the previous identification results (see Figs. 9a, 10a, and 11a). Furthermore, from Fig. 12c, it can be observed that despite the decrease in bridge stiffness, the time-varying frequencies of the VBI system can still be accurately captured by ridge extraction using TFRs of IMSST.

Over the years, the vehicle's suspension system could experience corrosion that leads to stiffness loss. In this scenario, a 9% stiffness loss ($k_1' = k_2' = 0.91k_1 = 0.91k_2$) was considered, as estimated over a 15 year period according to Ref. [48]. Similar results can be observed when using FFT and the presented method, as shown in Figs. 12b and d. Due to the decrease in suspension stiffness, the vehicle's original frequencies change to $f_v^{0\prime} = 4.330$ Hz and $f_p^{0\prime} = 7.636$ Hz. However, due to the interaction between the vehicle and the bridge, the identified frequencies are $f_v' = 4.444$ Hz and $f_p' = 7.629$ Hz, highlighting the limitations of FFT in identifying the time-varying characteristics of the VBI system. When IMSST and ridge extraction are utilized, Fig. 12d confirms that the presented method remains effective even with decreased vehicle suspension stiffness. Thus, while changes in bridge and vehicle stiffness do affect the system's frequencies, they do not significantly impact the time-varying frequency identification using the presented method.

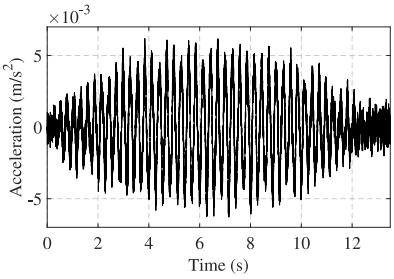

(a) Accelerations with 20% noises

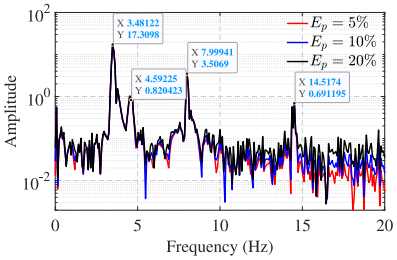

(b) FFT with different levels of noises

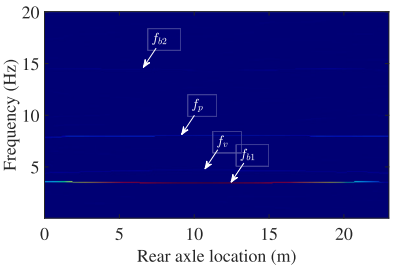

(c) TFRs using IMSST with 20% noises

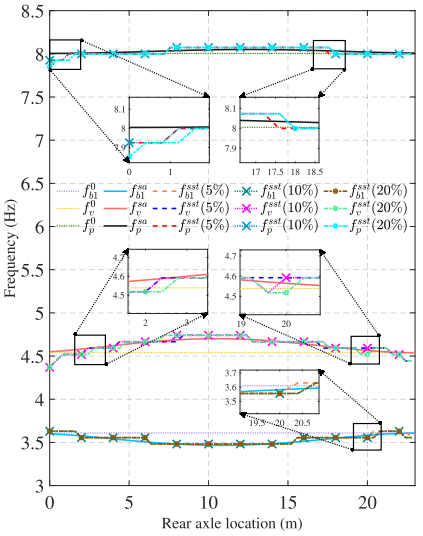

(d) Ridge extraction with different levels of noises

Fig. 13. Frequency identification of the VBI system using vehicle accelerations with different levels of noises.

3.4.5. Effect of environmental noises

In real-world engineering applications, it is inevitable to collect environmental noises when accelerometers are used to record vibration data from vehicles. In this section, Gaussian white noises are introduced to the recorded accelerations of the vehicle, as represented by Eq. (38) [14].

$$\ddot{z}_v^p = \ddot{z}_v + E_p N_s \sigma_{\ddot{z}_v} \tag{38}$$

where the contaminated vertical accelerations of the vehicle are denoted as $\ddot{z}_v^p$, while the vehicle's raw vertical vibration data without any noise is represented by $\ddot{z}_v$. E_p denotes the level of additional noise; N_s represents the standard normal distribution. $\sigma_{\ddot{z}_v}$ is the standard deviation of the vehicle's vertical accelerations. Other parameters of the vehicle and bridge are the same as described in Section 3.2. The vehicle's frequency spectrum, TFRs, and IFs have been plotted in Fig. 13. In this study, three different levels of environmental noise — 5%, 10%, and 20% — are selected to simulate various real-world engineering conditions. It should be noted that the 20% level is relatively high and has been employed in existing studies on the drive-by method [49].

As shown in Fig. 13a, when 20% noise is considered, the initial observation is that the time-domain signals of the vehicle appear more disordered due to the inclusion of noise in the collected accelerations. After transforming the vehicle's accelerations with different noise levels into the frequency domain, as shown in Fig. 13b, certain noisy peaks start to emerge in the frequency spectrum. With the increase in noise levels, these noisy peaks become more prominent, especially in the high-frequency ranges (e.g., 10–20 Hz). However, despite the increased complexity in the frequency spectrum, the frequencies associated with the VBI system can still be easily identified. Further analysis of the vehicle's TFRs using IMSST with 20% noise is shown in Fig. 13c. It is evident that the time-varying characteristics of both the vehicle and the bridge can still be effectively captured. The extracted IFs with different noise levels are plotted in Fig. 13d. It can be observed that the extraction of VBI frequencies in a low-frequency range is nearly unaffected, with only minor inconsistencies noticed (e.g., f_{b1} around 20 m). However, as the frequency range increases, such as in the identification of f_v, high noise levels tend to cause more significant inaccuracies in time-varying frequency identification (see around 2.4 m and 20 m). Similar effects are seen for the identification of f_p when the vehicle enters the bridge (see around

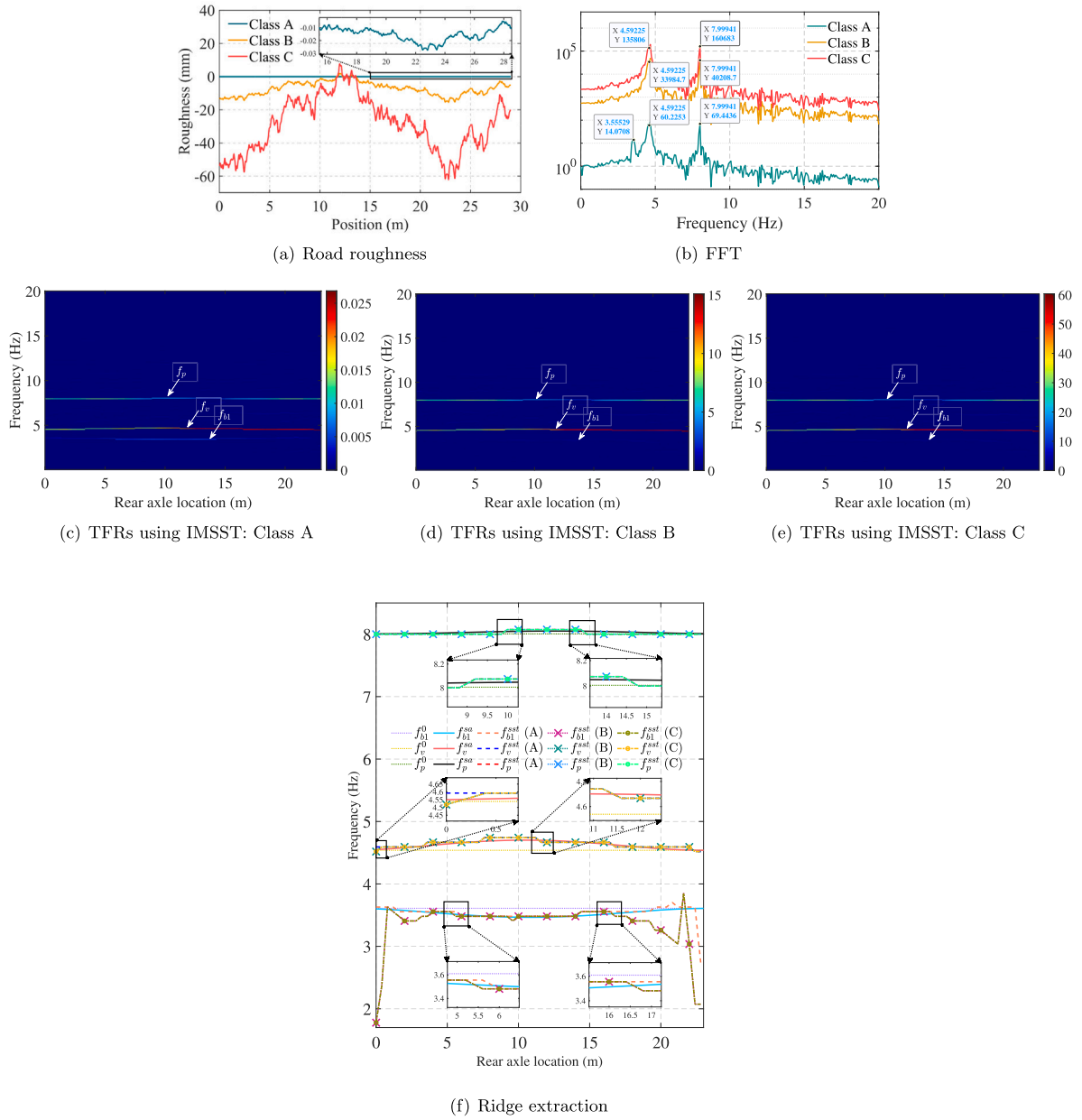

(a) Road roughness (b) FFT

(c) TFRs using IMSST: Class A (d) TFRs using IMSST: Class B (e) TFRs using IMSST: Class C

(f) Ridge extraction

Fig. 14. Frequency identification of the VBI system with road roughness of different classes.

1.2 m). Therefore, from the above analysis, it is clear that environmental noise levels do not greatly affect the identification of time-varying frequencies of the VBI system but have a more significant influence in the high-frequency range, especially when the noise level is high.

3.4.6. Effect of road roughness

Road roughness plays a significant role in accurately identifying the time-varying IFs of the VBI system, as it can overshadow the information from the bridge. In the drive-by method, road roughness is typically simulated using the power spectral density (PSD) function in ISO 8608 [50]. In this study, road roughness of Classes A, B, and C is investigated. In engineering scenarios, the contact between the vehicle and the bridge is typically an area rather than a single point [14]. To address this, a moving average filter with a window length of 30 is employed to smooth out the original point-wise road roughness, resulting in the road roughness profiles shown in Fig. 14a.

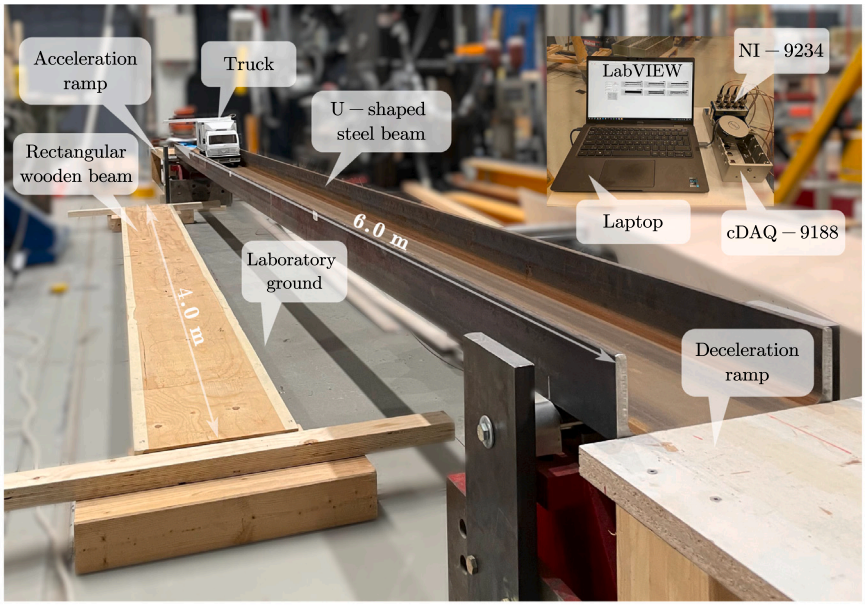

Fig. 15. Overview of laboratory experiments.

The frequency spectra of the vehicle's vertical accelerations under different road roughness conditions are shown in Fig. 14b. It is evident that road roughness stimulates the vehicle's frequencies to higher amplitudes in the spectrum. When the road roughness is very good (Class A), the fundamental frequency of the bridge is observable in the vehicle's accelerations. However, as the road roughness worsens (Classes B and C), the amplitudes of the vehicle's frequency-domain response increase significantly, making the bridge's frequency unidentifiable in the spectra while the vehicle's frequencies become more pronounced.

In the TFRs shown in Figs. 14c–e for different classes of road roughness, compared to Fig. 4b, frequencies f_v and f_p become more prominent, whereas f_{b1} weakens and f_{b2} cannot be observed. Fig. 14f shows the IF identification results using IMSST and ridge extraction. It is clear that when the road roughness is very good (Class A), the bridge's time-varying frequency can be extracted but with lower accuracy compared to that in Fig. 4c. For poorer road roughness, the ability to capture the bridge's IF decreases, especially when the vehicle enters and leaves the bridge. This is because at the moment the vehicle starts to enter the bridge, the vehicle's response contains little information about the bridge, being mostly excited by road roughness rather than bridge vibrations. Moreover, because the accelerations are collected from the vehicle itself, the identification of time-varying f_v and f_p is not affected. Based on these findings, it can be concluded that road roughness amplifies the frequency amplitudes of the vehicle, thereby diminishing the bridge's information in the spectrum of vehicle accelerations.

4. Laboratory experiments

To validate the proposed approach for identifying the time-varying frequencies of the VBI system using the drive-by method and IMSST, a series of laboratory experiments were conducted at the structural laboratory of Aalto University. These experiments first involved the use of a simply supported U-shaped steel beam (USB) and a scaled truck. Additionally, a rectangular wooden beam (RWB) was employed to explore the effectiveness of the method on bridges of different masses. An overview of the experimental setup is shown in Fig. 15. Further details regarding the experimental procedures will be provided in the subsequent sections.

4.1. Scaled truck model

In the laboratory experiments, we used a meticulously scaled two-axle truck (Tamiya Mercedes-Benz 1850L) to simulate real vehicles in engineering, as shown in Fig. 16a. The model was manufactured by Tamiya with a scale ratio of 1:14. In the experiments, three masses were sequentially added to the truck, resulting in truck masses of 5.357, 7.361, and 9.366 kg. The trucks with these masses are labeled as T1, T2, and T3, respectively, and T1 is shown in Fig. 16b. To collect the accelerations of the truck during its passage on the bridge, three accelerometers typed 352C03 from the PCB company were installed on its body, rear axle, and front axle, as shown in Figs. 16b and c. As described in Section 3.2, as both the vertical and rotational accelerations are capable of capturing the time-varying frequencies of the VBI system, only the vertical accelerations of the vehicle body (as referred to Fig. 16b) were recorded. From the bottom view of the truck, it can be observed that the truck has a suspension system, connecting shaft, engine, etc. The truck is operated using a remote control, as shown in Fig. 16a. It is important to note that due to manual control, the vehicle does not move in a strictly straight line during the experiment. Additionally, the speed of the vehicle varies

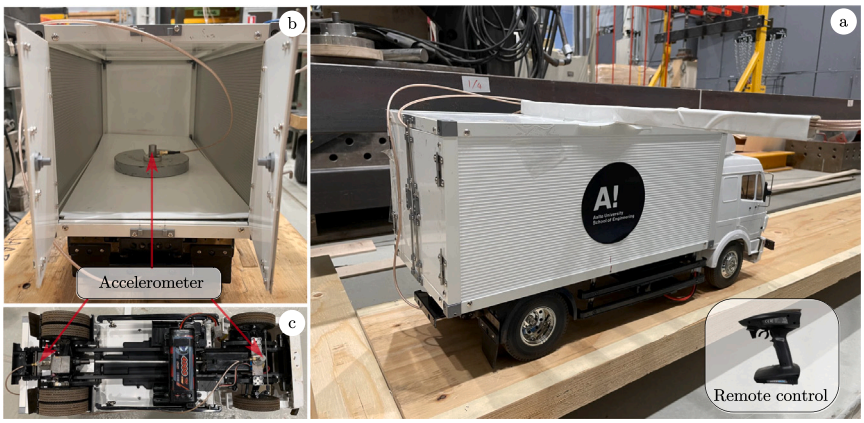

Fig. 16. Scaled truck model.

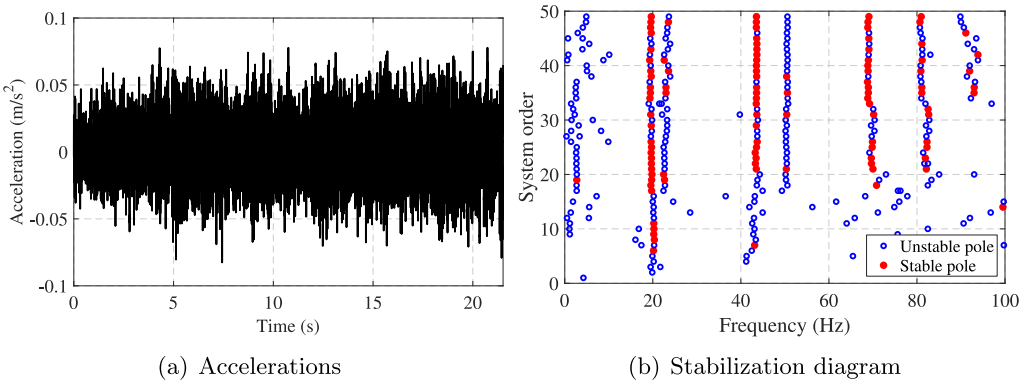

Fig. 17. Body responses of the T1 vehicle passing on laboratory ground.

slightly throughout its passage. The accelerations are then collected using input modules of NI-9234, a chassis of cDAQ-9188, and a laptop equipped with LabVIEW, as shown in Fig. 15. The sampling frequency of the accelerometers in the experiments is set at 1 kHz.

To obtain the frequencies of the vehicle, T1 is driven on the laboratory ground shown in Fig. 15. The body acceleration of the vehicle is shown in Fig. 17a. Then, the data-driven Stochastic Subspace Identification (SSI) method is employed for the vehicle's frequency identification. The stability criteria are set as 1% for eigenfrequencies, 5% for damping ratios, and 98% for the modal assurance criterion (MAC). The maximum system order is set to 50, and the number of block rows in the block Hankel matrix is 80. The stabilization diagram is shown in Fig. 17b, and the T1 vehicle's frequencies, f_{v1}^0 and f_{v2}^0, are estimated to be 19.708 Hz and 43.528 Hz, respectively. To investigate the time-varying characteristics of the VBI system, the passing speed of the vehicle is intentionally kept slow, with an average value of 0.11 m/s.

4.2. Beam models

The experiment utilized two beams, namely the USB and RWB, as shown in Fig. 15. The USB has a total length of 6.0 m, with 0.15 m reserved for each support, resulting in a span length of 5.7 m. The beam's cross-sectional area is 5660 mm^2 and its mass is 248.64 kg. Therefore, the vehicle–bridge mass ratio between T1 and the USB is 2.155%. To maintain a constant speed as the vehicle passes the USB, acceleration and deceleration ramps are employed at both ends. On the other hand, the RWB has a length of 4.0 m and a span length of 3.71 m. Its cross-sectional width and height are 0.295 m and 0.045 m, respectively. It has a mass of 25.2 kg, resulting in a vehicle–bridge mass ratio of 21.257% between T1 and the RWB.

To obtain the original frequency of the bridges, namely $f_{bi,S}^0$ or $f_{bi,W}^0$, impulse excitations generated by a modal hammer are utilized when there are no vehicles on the bridge. In addition, two accelerometers are installed at the 1/3-span positions of the two beams to measure their vibrations. The accelerometers on bridges serve two purposes: first, to determine the original frequencies of the bridges without the presence of trucks using impulse excitations; second, to record the accelerations of the beams during the passage of a truck and compare the time-varying frequency identification results from the beam vibrations to that obtained from vehicle responses. When the impulse excitations are applied, the time-domain accelerations and frequency spectra of the beams are

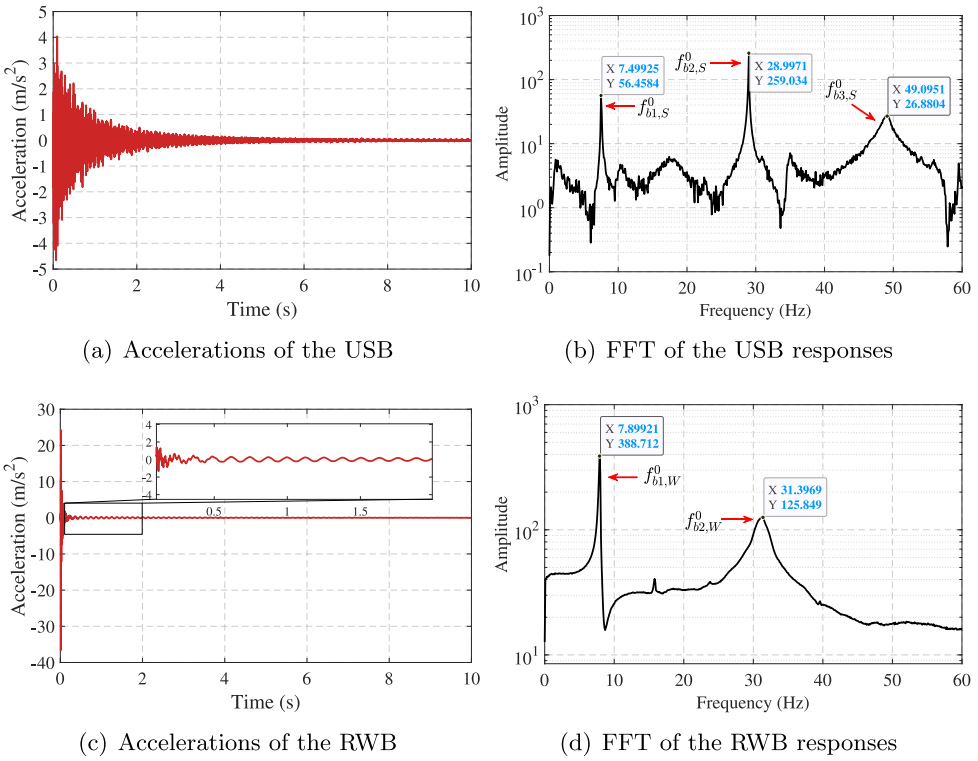

(a) Accelerations of the USB (b) FFT of the USB responses

(c) Accelerations of the RWB (d) FFT of the RWB responses

Fig. 18. Bridge responses under impulse excitations.

shown in Fig. 18. Based on Figs. 18b and d, it can be observed that the first three original frequencies of the USB, denoted as $f^0_{b1,S}$ to $f^0_{b3,S}$, are 7.499, 28.997, and 49.095 Hz, respectively, without considering the VBI effects. Here, the subscript S indicates that these frequencies belong to the steel beam. As for the RWB, its first two original frequencies, $f^0_{b1,W}$ and $f^0_{b2,W}$, are 7.899 and 31.397 Hz, respectively, without any passing vehicles, where the symbol W denotes wood. To validate the findings discussed in Section 3.3 regarding the vehicle–mass ratio, we deliberately maintained a narrow difference between the first two frequencies of the USB and RWB, resulting in a closely matched vehicle–bridge frequency ratio.

In this experiment, a relatively smooth road roughness is used compared to that of a real bridge. The vehicle excitations primarily come from the patterns of its rubber tires, which could be a potential method to simulate the effects of good road roughness in laboratory experiments [16]. It means that at the contact point between the vehicle and beams, the contact-point response includes the bridge's displacement, roughness of the tire, as well as road profile.

4.3. Results and discussions

4.3.1. Case 1: Basic study

When the T1 vehicle is driven at the speed v to pass the USB, the frequency spectrum of its body is shown in Fig. 19a. As mentioned in the previous section, accelerometers are also installed on the USB to record its vibrations during the passage of the vehicle. Fig. 19b displays the frequency spectrum of the bridge's forced vibrations caused by the vehicle's passage. We can see that the first two frequencies of the bridge, $f_{b1,S}$ and $f_{b2,S}$, can be clearly identified. However, the frequencies of the vehicle cannot be discerned from the bridge's frequency spectrum. Additionally, based on the findings in Fig. 17, it is evident that the frequencies of the vehicle can be identified from its vibrations. However, it is important to note that the above results obtained through direct FFT do not capture the time-varying characteristics of the VBI system. Therefore, the IMSST technique is employed to analyze the vibrations of the vehicle body and USB, as shown in Figs. 19c and d. The window length is selected as 12288.

From the direct measurement of the bridge vibrations, it can be clearly observed that the fundamental frequency of the bridge decreases when a vehicle passes over it, while the variation in its second frequency is not clear. Furthermore, we can observe that the decrease in the bridge's fundamental frequency can also be detected in the vehicle's responses, as shown in Fig. 19c. Additionally, the TFRs reveal the variation in the vehicle's first frequency. The ridge extraction results of $f_{b1,S}$ from the TFRs of both the vehicle and the bridge's responses are plotted in Fig. 19e. We can see that the time-varying frequency of the bridge during the VBI process can be accurately captured by the drive-by vehicle. However, when the vehicle enters or leaves the bridge, the bridge's fundamental frequency is not as well captured by the vehicle. This is because the vehicle begins to collect bridge vibrations only when it enters the bridge, and it stops collecting bridge vibrations once it leaves the bridge.

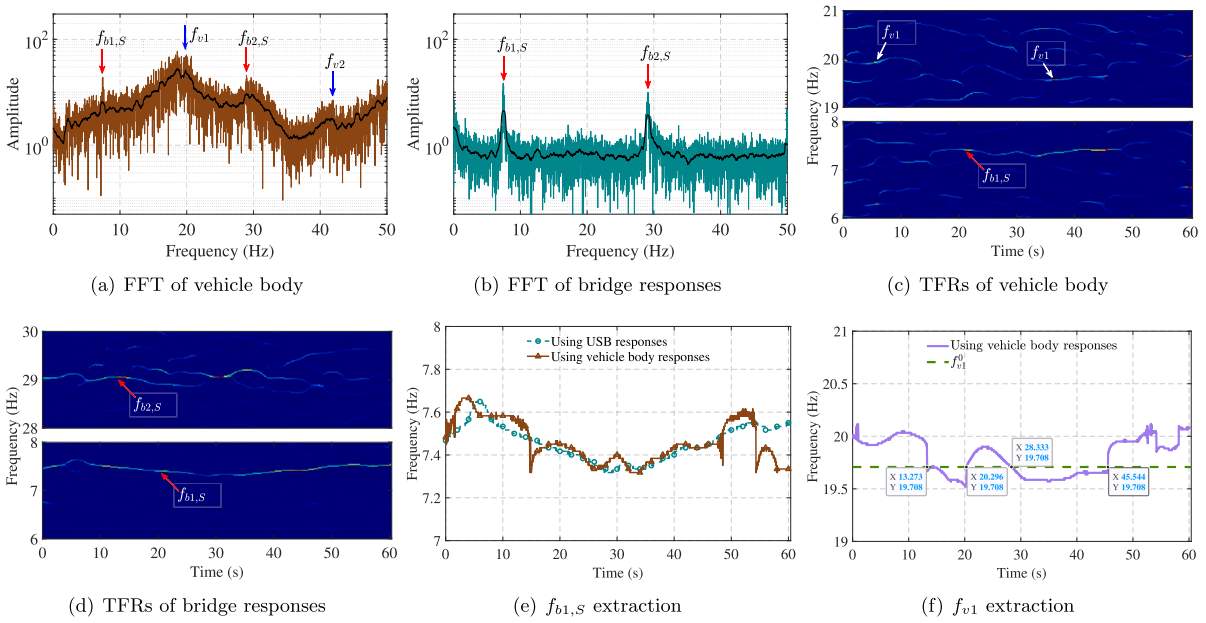

(a) FFT of vehicle body (b) FFT of bridge responses (c) TFRs of vehicle body

(d) TFRs of bridge responses (e) $f_{b1,S}$ extraction (f) f_{v1} extraction

Fig. 19. Results using body responses of the T1 vehicle and USB.

Additionally, from the identification results of the vehicle's first frequency f_{v1} as shown in Fig. 19f, we can see that it increases to around 20 Hz when the vehicle enters and leaves the bridge, compared to its original one f_{v1}^0 without VBI. Similar increases can also be observed when the vehicle passes the bridge (20.3–28.3 s). However, slight decreases can also be noticed during the vehicle's passage (13.3–20.3 s and 28.3–45.5 s). Therefore, it can be seen that the vehicle's frequency exhibits both increases and slight decreases in laboratory tests during the VBI process, i.e., fluctuations around f_{v1}^0. Since the bridge's frequency is of interest to engineers, subsequent sections will focus on analyzing the time-varying frequencies of the bridge. Unless stated otherwise, the parameters used will remain the same as in this section.

4.3.2. Case 2: Study on sensor positions

In the current research on the drive-by method, accelerometers are commonly attached to either the vehicle body or its axles [12,14]. In this experiment, we placed three sensors on the vehicle body and the front and rear axles individually. Upon the vehicle's passage, the vibrations from all three positions are simultaneously collected. The frequency spectra of the front and rear axles are plotted in Figs. 20a and b, respectively.

Upon observations, it is evident that the utilization of front axle responses leads to less distinguishable frequencies of the bridge compared to using vehicle body responses. The fundamental frequency of the bridge and vehicle frequencies are overshadowed by noisy peaks. Additionally, Fig. 20b shows that when the accelerations of the rear axle are utilized, the fundamental frequency of the bridge can still be observed. However, compared to Fig. 19a where vehicle body responses are used, the prominence of the bridge's fundamental frequency peak diminishes. The above results can be attributed to the susceptibility of the axle responses. As the vehicle and bridge are contacted by wheels that are directly connected to the axles, the axle responses are more prone to being influenced by road roughness. On the other hand, the vehicle body vibrates freely during passage and is not as strongly affected by road roughness. Therefore, in engineering applications involving the extraction of bridge information from vehicle vibrations, it is recommended to utilize the vehicle body's responses. Alternatively, the responses of the heavier axle can be considered.

To investigate the time-varying frequencies extracted from vehicle axle responses, Fig. 20c plots the TFRs of its rear axle vibrations. Although the bridge's fundamental frequency becomes weaker, its variation remains distinguishable. However, the road roughness significantly affects the vehicle's frequency f_{v1} in the high-frequency range, albeit with some observable traces. By employing ridge extraction, we can still identify the time-varying bridge frequency $f_{b1,S}$ from the vehicle's rear axle responses, as shown in Fig. 20d. However, the effects of entering and leaving the bridge become more remarkable.

4.3.3. Case 3: Study on vehicle mass

The variation of the bridge's frequency during the VBI process can be influenced by the mass of the vehicle. This is determined by the ratio of the vehicle–bridge mass ratios, as illustrated in Fig. 8. In this section, we will consider two vehicles, T2 and T3, with different masses as mentioned in Section 4.1. The vehicle/bridge mass ratios for T2 and T3 are 2.961% and 3.767%, respectively. Due to manual operations, the passing times are slightly different. The frequency spectrum, TFRs generated by the IMSST, and ridge extraction results of the vehicle body responses are shown in Fig. 21.

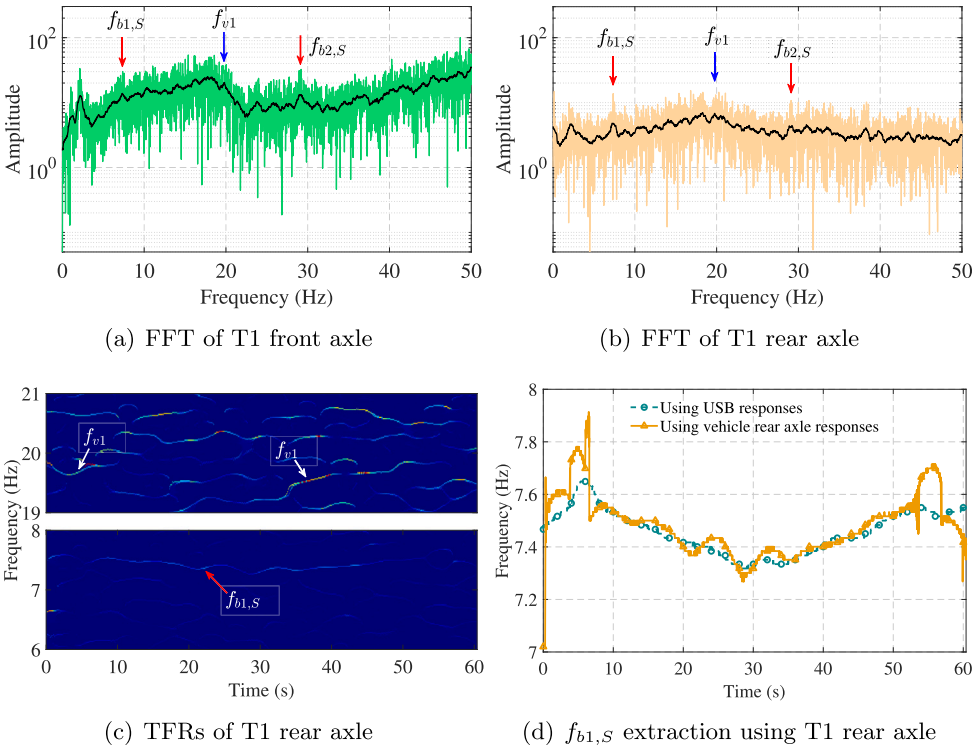

(a) FFT of T1 front axle (b) FFT of T1 rear axle

(c) TFRs of T1 rear axle (d) $f_{b1,S}$ extraction using T1 rear axle

Fig. 20. Results using responses of T1 vehicle axles.

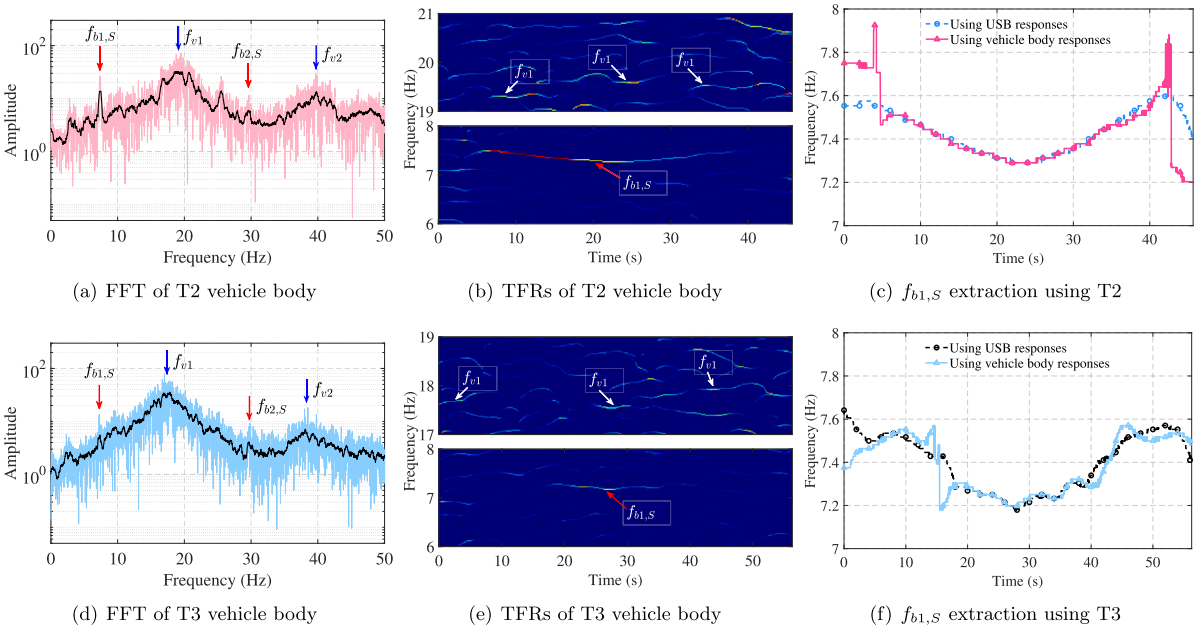

(a) FFT of T2 vehicle body (b) TFRs of T2 vehicle body (c) $f_{b1,S}$ extraction using T2

(d) FFT of T3 vehicle body (e) TFRs of T3 vehicle body (f) $f_{b1,S}$ extraction using T3

Fig. 21. Results using body responses of vehicles with different masses.

From Figs. 21a and d, we can see that the frequencies of the vehicle, f_{v1} and f_{v2}, have decreased due to the increase in vehicle mass. Additionally, the frequencies of the bridge can be observed from the frequency spectra of the vehicles. The TFRs obtained for the vehicle body responses using IMSST, as plotted in Figs. 21b and e, capture the decrease in vehicle frequencies. Moreover, the traces for the bridge's fundamental frequency are clearly identifiable. The extraction of ridges from the TFRs reveals that the

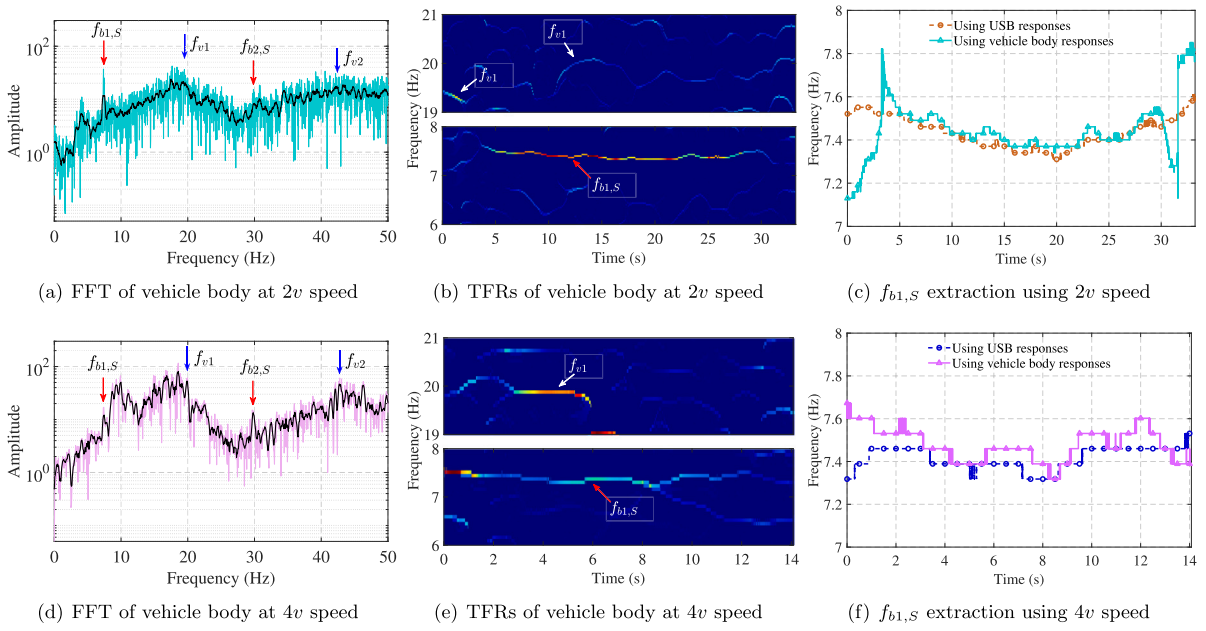

(a) FFT of vehicle body at $2v$ speed (b) TFRs of vehicle body at $2v$ speed (c) $f_{b1,S}$ extraction using $2v$ speed

(d) FFT of vehicle body at $4v$ speed (e) TFRs of vehicle body at $4v$ speed (f) $f_{b1,S}$ extraction using $4v$ speed

Fig. 22. Results using body responses of the T1 vehicle at different speeds.

time-varying frequency of the USB can be identified from the responses of vehicles with varying masses. Furthermore, upon closer examination of the variation in the bridge's fundamental frequency, it is observed that there is a larger decrease in $f_{b1,S}$ with an increase in vehicle mass. In comparison to Fig. 19e, where the T1 vehicle is used, the bridge's frequency at its midpoint has decreased to 7.290 Hz and 7.179 Hz for T2 and T3 vehicles, respectively. However, this slight decrease cannot be captured by a simple FFT but can be identified from the drive-by vehicle's responses. Furthermore, we can still notice the inaccuracy of bridge frequency capture at the beginning and leaving periods, especially for the T2 vehicle.

4.3.4. Case 4: Study on vehicle speed

In Section 3.4.1, numerical simulations were conducted to analyze the effects of vehicle speeds. For experimental validation, two higher speeds, approximately $2v$ and $4v$, were considered. As introduced in Section 3.4.1, high speed will make the passing time shorter and decrease the frequency resolution in TFRs, resulting in challenges in acquiring the time-varying characteristics of frequencies. The section utilizes a shorter window length of 8192 to increase the time resolution [51]. The time-varying frequency identification results of the VBI system can be found in Fig. 22.

Upon comparing Figs. 22a and d, it becomes apparent that the frequency resolution declines as the vehicle speeds increase. Furthermore, the frequency spectra clearly show that the first two frequencies of the USB remain identifiable. However, it is also noticeable that when the vehicle speed reaches $4v$, more interfering peaks emerge. This occurrence can be attributed to the impact of road roughness. As the speed increases, the collision between the tire and the uneven road roughness generates an impulsive force that transfers more energy to the bridge, resulting in a stronger VBI response. Simultaneously, a greater amount of information regarding road roughness is transmitted to the vehicle, exacerbating the disruption caused by road irregularities and diminishing the bridge's frequency identifiability. At the same time, the high speed of the vehicle leads to a shorter passage time, which results in less bridge information being collected. This, in turn, hampers the identification of time-varying bridge frequencies. The TFRs of the T1 vehicle's body responses are plotted in Figs. 22b and d, and the ridge extraction results of $f_{b1,S}$ are shown in Figs. 22c and f when employing the higher speeds $2v$ and $4v$. We can see that due to the decrease in frequency resolution, the time-varying frequencies of the bridge captured from the bridge itself and from the vehicle are less matched, especially when the $4v$ speed is utilized. However, the overall trend of variation can still be captured. In engineering applications where the time-varying characteristics of the bridge are of interest and the vehicle's vibrations are utilized, the speed cannot be too high. Otherwise, variations of frequencies of the VBI system will be less trappable [22].

4.3.5. Case 5: Study on bridge mass

The use of vehicles and USB in the previous sections does not result in significant variation in bridge frequencies during vehicle passage, as demonstrated in Fig. 7c. In engineering practice, this mass ratio can exceed 10% [24]. In this section, the analysis is performed using RWB. As mentioned in Section 4.2, the first two original frequencies of USB and RWB are set to be close to each other to keep a relatively constant vehicle–bridge frequency ratio. When the T1 vehicle is used with RWB, the vehicle–bridge mass ratio becomes 21.257%. Additionally, as observed in the previous sections, the fundamental frequency of the bridge cannot be accurately tracked when the vehicle enters and leaves the bridge. Specifically, when the vehicle starts to be driven, its front wheels

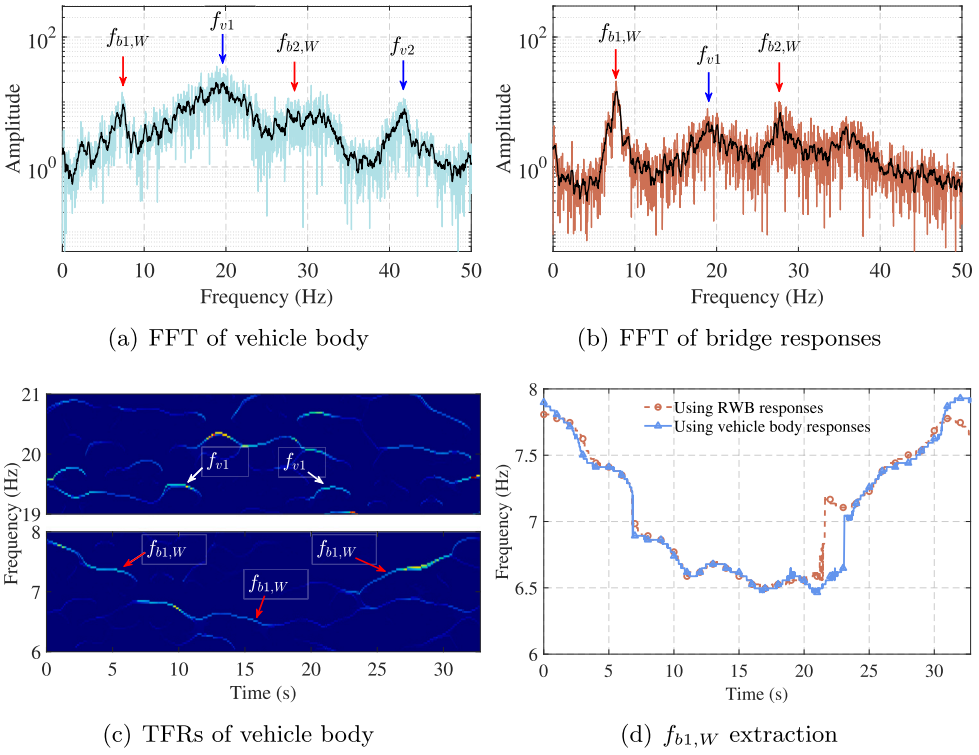

Fig. 23. Results using body responses of the T1 vehicle passing the RWB.

are already on the bridge, and only a short acceleration ramp is used for its rear wheels. The time-varying frequency identification results of the VBI system are presented in Fig. 23.

Figs. 23a and b demonstrate that both the bridge's frequencies and the vehicle's frequencies can be identified from the vehicle's body responses. Additionally, the bridge's responses reveal that not only can the bridge's frequencies be observed, but the vehicle's first frequency is also observable. This implies that the vehicle's dynamic information can also be transferred to the bridge during their interaction. The TFRs of the vehicle's responses are shown in Fig. 23c. We can see that the bridge's time-varying fundamental frequency can be well-tracked. The extraction ridges from the vehicle responses and bridge responses are displayed in Fig. 23d, showing a strong correlation even in cases where the bridge's fundamental frequency experiences a significant decrease (approximately 1.5 Hz decrease when the vehicle passes the bridge's midpoint). These findings align with the results shown in Fig. 7c, which indicate that a large vehicle–bridge mass ratio leads to a sharp decrease in the bridge's fundamental frequency. As a result, the proposed approach of utilizing vehicle responses to track the time-varying characteristics of the VBI system proves to be effective and is recommended in engineering applications for some downstream work, such as frequency-based bridge condition assessment.

4.3.6. *Evaluation of time-varying bridge frequency extraction from vehicle responses*

The preceding sections highlight that the proposed approach can effectively extract the time-varying fundamental frequency of a bridge from the responses of passing vehicles in various cases. To assess the method's effectiveness in different scenarios, this section introduces a novel index, termed the T-DTW distance, to evaluate the accuracy of identifying time-varying frequencies from vehicle responses. Let $\mathbf{f}_{bk}^{V} = [f_{bk,1}^{V}, \ldots, f_{bk,N}^{V}]$ represent the kth time-varying frequency sequence obtained from the vehicle, and $\mathbf{f}_{bk}^{B} = [f_{bk,1}^{B}, \ldots, f_{bk,N}^{B}]$ denote the corresponding frequency sequence from the bridge. Considering $\mathbf{f}_{bk}^{B}$ as the ground truth, the T-DTW distance γ_{Tk} can be calculated using Eqs. (39) and (40) .

$$\gamma_{Tk} = \gamma(i,j)/T_t \cdot f_s \cdot 100\% \tag{39}$$

$$\gamma(i,j) = \sqrt{(f_{bk,i}^{V} - f_{bk,j}^{B})^2} + \min\{\gamma(i-1,j-1), \gamma(i-1,j), \gamma(i,j-1)\} \tag{40}$$

where $\gamma(i,j)$ means the cumulative distance. $f_{bk,i}^{V}$ represents the ith point of the kth order bridge frequency sequence extracted from vehicle responses, while $f_{bk,j}^{B}$ denotes the jth frequency point extracted from bridge responses. The sampling frequency is represented by f_s, and T_t is the vehicle's passing time. It is important to note that the passing time of the vehicle can vary in engineering scenarios, but the above equation eliminates this influence. For comparison, several commonly used criteria such as

Table 2
Evaluation of $\mathbf{f}_{b1}^{V}$ identified from response vehicles.

Case	Case 1	Case 2	Case 3.1	Case 3.2	Case 4.1	Case 4.2	Case 5
Vehicle mass	T1	T1	T2	T3	T1	T1	T1
Sensor position	Body	Rear axle	Body	Body	Body	Body	Body
Speed	v	v	v	v	$2v$	$4v$	v
Bridge	USB	USB	USB	USB	USB	USB	RWB
ED_1	16.4027	16.6694	21.3436	15.3414	21.9809	11.2837	23.7219
MAC_1	0.9999	0.9999	0.9998	0.9999	0.9997	0.9999	0.9997
R_1^2	0.3483	0.3269	0.0088	0.7530	−1.8761	−2.3237	0.9158
γ_{T1}	2.08%	2.34%	3.80%	1.71%	4.92%	3.55%	1.94%

Euclidean distance (ED), MAC value, and R-squared (R^2) are calculated. These criteria for the kth extracted frequency sequence can be obtained using Eq. (41). The evaluation values for the extracted $\mathbf{f}_{bk}^{V}$ in different cases have been listed in Table 2.

$$\mathrm{ED}_k = \sqrt{\sum_{i=1}^{N}(f_{bk,i}^{B}, f_{bk,i}^{V})};\ \mathrm{MAC}_k = \frac{\left|(\mathbf{f}_{bk}^{V})^T(\mathbf{f}_{bk}^{B})\right|^2}{\left|(\mathbf{f}_{bk}^{V})^T(\mathbf{f}_{bk}^{V})\right|\left|(\mathbf{f}_{bk}^{B})^T(\mathbf{f}_{bk}^{B})\right|};\ R_k^2 = 1 - \frac{\sum_{i=1}^{N}(f_{bk,i}^{B} - f_{bk,i}^{V})^2}{\sum_{i=1}^{N}(f_{bk,i}^{B} - \bar{f}_{bk}^{B})^2}. \tag{41}$$

For different cases, we can observe that when ED is used, the evaluation values in cases 1–4.1 and 5 are close. Take cases 3.1 and 4.1 as examples, and the qualities of time-varying frequency values extracted from the vehicle are different (see Figs. 21c and 22c), especially when it passes the intermediate part of the bridge. However, their ED values are close to each other. Additionally, when the MAC values are utilized, we can see that all criteria fall between 0.9997 and 0.9999, which is very close to 1.0. This indicates that the frequency values extracted from the vehicle match the ones from the bridge quite well. However, there are clear differences observed for different cases. When R^2 is used, cases 4.1 and 4.2 have negative evaluations, indicating a very poor extraction. However, in case 4.1, the extracted frequency values from the vehicle can capture the trend of the bridge frequency decrease. The above findings indicate the failure of these traditional criteria.

DTW is a method used to assess the similarity in shape between two time-dependent sequences. From Fig. 19a, we can see that the time–frequency variations captured by the vehicle and the bridge may not be time-aligned (see 0–10 s), even though they have a similar trend. DWT can be a good candidate to evaluate local similarity between two sequences. Furthermore, due to the difference in the passing time of various vehicle runs, the concept of T-DTW is proposed to remove the influence of passing time. For T-DTW values, a low percent near zero means good time-varying frequency extraction. The evaluation values γ_{T1} have been listed in Table 2. We can see that compared to traditional criteria, the proposed T-DTW values are more effective in assessing the extracted time-varying bridge frequencies. For instance, there is a 1.12% difference between cases 3.1 and 4.1 instead of a similar distance by the ED. Figs. 21c and 22c show that higher T-DTW values for evaluating cases 3.1 and 4.1 are mainly attributed to inaccuracies in the frequency capture during the vehicle's entering and leaving times. Furthermore, case 4.1 demonstrates a poorer matching degree during the intermediate time compared to case 3.1, and therefore a poorer T-DTW value is given. Consequently, the evaluation of T-DTW values proves to be meaningful and effective. In this work, the authors find that T-DTW values lower than 5% can represent a good match between the identified time-varying bridge frequencies from the vehicle and the bridge itself, and thus recommend it be utilized for frequency extraction evaluation in other future studies.

5. Conclusions and future work

This paper explores the time-varying frequencies of the VBI system, which consists of a two-axle vehicle and a simply supported bridge. New semi-analytical solutions for the system are derived and validated through numerical simulations. Furthermore, the IMSST method is presented to generate clear TFRs that can accurately track the frequency variations of the VBI system using vehicle responses. To demonstrate the effectiveness of the proposed strategy, laboratory experiments are conducted using a scaled model truck and two beams, and a novel index, called T-DTW, is recommended for the evaluation of time-varying bridge frequency extraction using the drive-by method. Several concluding remarks are drawn below.

(1) The proposed semi-analytical solution for time-varying frequencies of the VBI system is derived, and the frequency variations of the two-axle vehicle and bridge can be captured by TFRs generated by IMSST in numerical simulations.
(2) According to numerical simulations when the two-axle vehicle is employed, both the vertical and pitching frequencies need to be considered for the resonance phenomenon between the vehicle and bridge. When the bridge's fundamental frequency is slightly higher than that of the vehicle, the bridge's fundamental frequency increases greatly during the interaction. Instead, if it is marginally lower than the vehicle's frequencies, the bridge's fundamental frequency decreases much during the passage.
(3) High vehicle speed decreases the vehicle's passing time, making the frequency resolution limited to capture frequency variations of the VBI system. Damping in the system will inversely influence the identification of the system's time-varying frequencies. Experimental results show that vehicle body responses facilitate the identification of time-varying bridge frequencies compared to that of vehicle axles.
(4) Compared to traditional methods, the proposed T-DTW index can better evaluate the time-varying bridge frequency extraction results from vehicle responses and is suggested for examining prospective methods.

Even though time-varying characteristics of the VBI system are studied in this work, engineering applications typically involve more influential factors such as multiple-axle vehicles and heavy ongoing traffic. Furthermore, 3D modeling that can better represent an engineering VBI system will be explored. The proposed IMSST-based method shows great potential in tracking bridge frequency variation using the drive-by method. Our future studies will check the above influential factors and time-varying characteristics of 3D VBI systems.

CRediT authorship contribution statement

Zhenkun Li: Writing – review & editing, Writing – original draft, Visualization, Validation, Software, Methodology, Investigation, Formal analysis, Data curation, Conceptualization. **Yifu Lan:** Writing – review & editing, Validation, Investigation. **Kun Feng:** Writing – review & editing, Software. **Weiwei Lin:** Writing – review & editing, Supervision, Project administration, Funding acquisition.

Declaration of competing interest

The authors declare that they have no known competing financial interests or personal relationships that could have appeared to influence the work reported in this paper.

Data availability

Data will be made available on request.

Acknowledgments

This research is financially sponsored by the Jane and Aatos Erkko Foundation in Finland (Decision number: 210018) and Aalto University (research project funding in ENG 2022). K. Feng is supported by the Engineering and Physical Sciences Research Council (EPSRC) Prosperity Partnerships Project (EPSRC Reference EP/S036695/1). We acknowledge the provision of facilities and technical support in the Department of Civil Engineering and the Solid Mechanics Laboratory in the Department of Mechanical Engineering at Aalto University. The calculations presented above were partly performed using computer resources within the Aalto University School of Science "Science-IT" project.

References

[1] P. Negi, R. Kromanis, A.G. Doé, K.M. Wijnberg, Structural health monitoring of inland navigation structures and ports: A review on developments and challenges, Struct. Health Monit. 23 (1) (2023) 605–645, http://dx.doi.org/10.1177/14759217231170742.
[2] European Commission, Joint Research Centre, A. Tsakalidis, A. Ortega Hortelano, M. Grosso, M. Balen, G. Haq, K. Gkoumas, F. Marques Dos Santos, F. Pekár, Research and Innovation in Bridge Maintenance, Inspection and Monitoring – A European perspective based on the Transport Research and Innovation Monitoring and Information System (TRIMIS), Publications Office, 2019, http://dx.doi.org/10.2760/719505.
[3] American Society of Civil Engineers, ASCE's 2021 report card: Bridges, ASCE(American Society of Civil Engineers), 2021.
[4] O. Avci, O. Abdeljaber, S. Kiranyaz, M. Hussein, M. Gabbouj, D.J. Inman, A review of vibration-based damage detection in civil structures: From traditional methods to machine learning and deep learning applications, Mech. Syst. Signal Process. 147 (2021) 107077, http://dx.doi.org/10.1016/j.ymssp.2020.107077.
[5] Y. An, E. Chatzi, S.H. Sim, S. Laflamme, B. Blachowski, J. Ou, Recent progress and future trends on damage identification methods for bridge structures, Struct. Control Health Monit. 26 (10) (2019) e2416, http://dx.doi.org/10.1002/stc.2416.
[6] C. Roberts, L.D. Avendaño Valencia, D. García Cava, Robust mitigation of EOVs using multivariate nonlinear regression within a vibration-based SHM methodology, Mech. Syst. Signal Process. 208 (2024) 111028, http://dx.doi.org/10.1016/j.ymssp.2023.111028.
[7] K. Feng, A. González, M. Casero, A kNN algorithm for locating and quantifying stiffness loss in a bridge from the forced vibration due to a truck crossing at low speed, Mech. Syst. Signal Process. 154 (2021) 107599, http://dx.doi.org/10.1016/j.ymssp.2020.107599.
[8] M.Z. Sarwar, D. Cantero, Probabilistic autoencoder-based bridge damage assessment using train-induced responses, Mech. Syst. Signal Process. 208 (2024) 111046, http://dx.doi.org/10.1016/j.ymssp.2023.111046.
[9] A. Malekjafarian, R. Corbally, W. Gong, A review of mobile sensing of bridges using moving vehicles: Progress to date, challenges and future trends, Structures 44 (2022) 1466–1489, http://dx.doi.org/10.1016/j.istruc.2022.08.075.
[10] Y.B. Yang, C.W. Lin, J.D. Yau, Extracting bridge frequencies from the dynamic response of a passing vehicle, J. Sound Vib. 272 (3–5) (2004) 471–493, http://dx.doi.org/10.1016/S0022-460X(03)00378-X.
[11] Y. Lan, Z. Li, K. Koski, L. Fülöp, T. Tirkkonen, W. Lin, Bridge frequency identification in city bus monitoring: A coherence-PPI algorithm, Eng. Struct. 296 (2023) 116913, http://dx.doi.org/10.1016/j.engstruct.2023.116913.
[12] H. Xu, Y.H. Liu, J. Chen, D.S. Yang, Y.B. Yang, Novel formula for determining bridge damping ratio from two wheels of a scanning vehicle by wavelet transform, Mech. Syst. Signal Process. 208 (2024) 111026, http://dx.doi.org/10.1016/j.ymssp.2023.111026.
[13] Y.B. Yang, J. Chen, H. Xu, Normalized formula for removing damping effect in recovering bridge mode shapes using a moving and a stationary vehicle, J. Sound Vib. 573 (2024) 118219, http://dx.doi.org/10.1016/j.jsv.2023.118219.
[14] Z. Li, Y. Lan, W. Lin, Indirect damage detection for bridges using sensing and temporarily parked vehicles, Eng. Struct. 291 (2023) 116459, http://dx.doi.org/10.1016/j.engstruct.2023.116459.
[15] Y. Lan, Z. Li, W. Lin, Physics-guided diagnosis framework for bridge health monitoring using raw vehicle accelerations, Mech. Syst. Signal Process. 206 (2024) 110899, http://dx.doi.org/10.1016/j.ymssp.2023.110899.
[16] R. Corbally, A. Malekjafarian, A deep-learning framework for classifying the type, location, and severity of bridge damage using drive-by measurements, Comput.-Aided Civ. Infrastruct. Eng. 39 (6) (2023) 852–871, http://dx.doi.org/10.1111/mice.13104.
[17] A. González, K. Feng, M. Casero, Effective separation of vehicle, road and bridge information from drive-by acceleration data via the power spectral density resulting from crossings at various speeds, Dev. Built Environ. 14 (2023) 100162, http://dx.doi.org/10.1016/j.dibe.2023.100162.

[18] X. Kong, C.S. Cai, B. Kong, Numerically extracting bridge modal properties from dynamic responses of moving vehicles, J. Eng. Mech. 142 (6) (2016) 04016025, http://dx.doi.org/10.1061/(asce)em.1943-7889.0001033.
[19] X. Jian, Y. Xia, L. Sun, Indirect identification of bridge frequencies using a four-wheel vehicle: Theory and three-dimensional simulation, Mech. Syst. Signal Process. 177 (2022) 109155, http://dx.doi.org/10.1016/j.ymssp.2022.109155.
[20] J. Zhang, T.H. Yi, C.X. Qu, Q. Han, Y.F. Wang, X.D. Mei, Experimental studies of extracting bridge mode shapes by response of a moving vehicle, J. Bridge Eng. 28 (11) (2023) 04023076, http://dx.doi.org/10.1061/JBENF2.BEENG-6243.
[21] Z. Li, W. Lin, Y. Zhang, Bridge frequency scanning using the contact-point response of an instrumented 3D vehicle: Theory and numerical simulation, Struct. Control Health Monit. 2023 (2023) 3924349, http://dx.doi.org/10.1155/2023/3924349.
[22] C. Tan, H. Zhao, E.J. OBrien, N. Uddin, C.-W. Kim, Exploring time-varying characteristics in drive-by bridge frequency extraction with the second-order synchrosqueezing transform, J. Bridge Eng. 28 (4) (2023) 04023010, http://dx.doi.org/10.1061/JBENF2.BEENG-5979.
[23] Z. Li, W. Lin, Y. Zhang, Drive-by bridge damage detection using mel-frequency cepstral coefficients and support vector machine, Struct. Health Monit. 22 (5) (2023) 3302–3319, http://dx.doi.org/10.1177/14759217221150932.
[24] J. Li, X. Zhu, S.S. Law, B. Samali, A two-step drive-by bridge damage detection using dual Kalman filter, Int. J. Struct. Stab. Dyn. 20 (10) (2020) 2042006, http://dx.doi.org/10.1142/S0219455420420067.
[25] D. Cantero, P. McGetrick, C.W. Kim, E. OBrien, Experimental monitoring of bridge frequency evolution during the passage of vehicles with different suspension properties, Eng. Struct. 187 (2019) 209–219, http://dx.doi.org/10.1016/j.engstruct.2019.02.065.
[26] R.G. Stockwell, A basis for efficient representation of the S-transform, Digit. Signal Process. 17 (1) (2007) 371–393, http://dx.doi.org/10.1016/j.dsp.2006.04.006.
[27] F. Auger, P. Flandrin, Improving the readability of time–frequency and time-scale representations by the reassignment method, IEEE Trans. Signal Process. 43 (5) (1995) 1068–1089, http://dx.doi.org/10.1109/78.382394.
[28] G. Yu, M. Yu, C. Xu, Synchroextracting transform, IEEE Trans. Ind. Electron. 64 (10) (2017) 8042–8054, http://dx.doi.org/10.1109/TIE.2017.2696503.
[29] I. Daubechies, J. Lu, H.T. Wu, Synchrosqueezed wavelet transforms: An empirical mode decomposition-like tool, Appl. Comput. Harmon. Anal. 30 (2) (2011) 243–261, http://dx.doi.org/10.1016/j.acha.2010.08.002.
[30] N. Mostafa, D. Di Maio, R. Loendersloot, T. Tinga, Extracting the time-dependent resonances of a vehicle–bridge interacting system by wavelet synchrosqueezed transform, Struct. Control Health Monit. 28 (12) (2021) e2833, http://dx.doi.org/10.1002/stc.2833.
[31] L. Tang, X.Q. Shang, T.L. Huang, N.B. Wang, W.X. Ren, An improved local maximum synchrosqueezing transform with adaptive window width for instantaneous frequency identification of time-varying structures, Eng. Struct. 292 (2023) 116543, http://dx.doi.org/10.1016/j.engstruct.2023.116543.
[32] Y. Xin, H. Hao, J. Li, Time-varying system identification by enhanced empirical wavelet transform based on synchroextracting transform, Eng. Struct. 196 (2019) 109313, http://dx.doi.org/10.1016/j.engstruct.2019.109313.
[33] Y.B. Yang, M.C. Cheng, K.C. Chang, Frequency variation in vehicle–bridge interaction systems, Int. J. Struct. Stab. Dyn. 13 (02) (2013) 1350019, http://dx.doi.org/10.1142/S0219455413500193.
[34] J. Li, X. Zhu, S.S. Law, B. Samali, Time-varying characteristics of bridges under the passage of vehicles using synchroextracting transform, Mech. Syst. Signal Process. 140 (2020) 106727, http://dx.doi.org/10.1016/j.ymssp.2020.106727.
[35] X. Zhu, Z. Zhang, J. Gao, B. Li, Z. Li, X. Huang, G. Wen, Synchroextracting chirplet transform for accurate IF estimate and perfect signal reconstruction, Digit. Signal Process. 93 (2019) 172–186, http://dx.doi.org/10.1016/j.dsp.2019.07.015.
[36] G. Yu, A multisynchrosqueezing-based high-resolution time–frequency analysis tool for the analysis of non-stationary signals, J. Sound Vib. 492 (2021) 115813, http://dx.doi.org/10.1016/j.jsv.2020.115813.
[37] Y. He, J.P. Yang, Using acceleration residual spectrum from single two-axle vehicle at contact points to extract bridge frequencies, Eng. Struct. 266 (2022) 114538, http://dx.doi.org/10.1016/j.engstruct.2022.114538.
[38] L. Guilbeau, The history of the solution of the cubic equation, Math. News Lett. 5 (4) (1930) 8–12, http://dx.doi.org/10.2307/3027812.
[39] F. Auger, P. Flandrin, Y.T. Lin, S. McLaughlin, S. Meignen, T. Oberlin, H.T. Wu, Time–frequency reassignment and synchrosqueezing: An overview, IEEE Signal Process. Mag. 30 (6) (2013) 32–41, http://dx.doi.org/10.1109/MSP.2013.2265316.
[40] G. Yu, Z. Wang, P. Zhao, Multisynchrosqueezing transform, IEEE Trans. Ind. Electron. 66 (7) (2018) 5441–5455, http://dx.doi.org/10.1109/TIE.2018.2868296.
[41] S. Meignen, T. Oberlin, P. Depalle, P. Flandrin, S. McLaughlin, Adaptive multimode signal reconstruction from timefrequency representations, Phil. Trans. R. Soc. A 374 (2065) (2016) 20150205, http://dx.doi.org/10.1098/rsta.2015.0205.
[42] R.A. Carmona, W.L. Hwang, B. Torresani, Characterization of signals by the ridges of their wavelet transforms, IEEE Trans. Signal Process. 45 (10) (1997) 2586–2590, http://dx.doi.org/10.1109/78.640725.
[43] D.H. Pham, S. Meignen, High-order synchrosqueezing transform for multicomponent signals analysis—with an application to gravitational-wave signal, IEEE Trans. Signal Process. 65 (12) (2017) 3168–3178, http://dx.doi.org/10.1109/TSP.2017.2686355.
[44] J.A. Li, D. Feng, A comparative study of vehicle–bridge interaction dynamics with 2D and 3D vehicle models, Eng. Struct. 292 (2023) 116493, http://dx.doi.org/10.1016/j.engstruct.2023.116493.
[45] Y.B. Yang, H. Xu, Z.L. Wang, K. Shi, Using vehicle–bridge contact spectra and residue to scan bridge's modal properties with vehicle frequencies and road roughness eliminated, Struct. Control Health Monit. 29 (8) (2022) e2968, http://dx.doi.org/10.1002/stc.2968.
[46] A. González, E.J. OBrien, P. McGetrick, Identification of damping in a bridge using a moving instrumented vehicle, J. Sound Vib. 331 (18) (2012) 4115–4131, http://dx.doi.org/10.1016/j.jsv.2012.04.019.
[47] A. González, K. Feng, M. Casero, The use of the forced frequency of a bridge due to a truck fleet for estimating stiffness losses at low speed, Appl. Sci. 12 (22) (2022) 11380, http://dx.doi.org/10.3390/app122211380.
[48] Y. Wang, C. Soutis, M. Yar, X. Zhou, Modelling corrosion effect on stiffness of automotive suspension springs, Mater. Des. Process. Commun. 1 (1) (2019) e25, http://dx.doi.org/10.1002/mdp2.25.
[49] Y.B. Yang, X.S. Hu, K. Shi, X.Q. Mo, B. Zhang, Z.L. Wang, H. Xu, Damage detection for constituents of track-bridge systems from driving component of vehicle-rail contact response, Eng. Struct. 259 (2022) 114143, http://dx.doi.org/10.1016/j.engstruct.2022.114143.
[50] ISO 8608, Mechanical Vibration-Road Surface Profiles-Reporting of Measured Data, second ed., International Organization for Standardization, Geneva, 2016, (2016-11-01).
[51] L. Cohen, Uncertainty principles of the short-time Fourier transform, in: Advanced Signal Processing Algorithms, Vol. 2563, International Society for Optics and Photonics, SPIE, 1995, pp. 80–90, http://dx.doi.org/10.1117/12.211427.